Available online at www.sciencedirect.com
ScienceDirect
Journal of Computational Physics 227 (2008) 3971–4001
JOURNAL OF COMPUTATIONAL PHYSICS
www.elsevier.com/locate/jcp

Finite volume schemes of very high order of accuracy for stiff hyperbolic balance laws

Michael Dumbser [a,*], Cedric Enaux [b], Eleuterio F. Toro [a]

[a] *Laboratory of Applied Mathematics, University of Trento, Via Mesiano 77, I-38100 Trento, Italy*
[b] *CEA – DIF, F-91680 Bruyères-Le-Châtel, France*

Received 31 January 2007; received in revised form 25 September 2007; accepted 10 December 2007
Available online 23 December 2007

Abstract

In this article, we propose a new class of finite volume schemes of arbitrary accuracy in space and time for systems of hyperbolic balance laws with *stiff* source terms. The new class of schemes is based on a three stage procedure. First a high-order WENO reconstruction procedure is applied to the cell averages at the current time level. Second, the temporal evolution of the reconstruction polynomials is computed *locally* inside each cell using the governing equations. In the original ENO scheme of Harten et al. and in the ADER schemes of Titarev and Toro, this time evolution is achieved via a Taylor series expansion where the time derivatives are computed by repeated differentiation of the governing PDE with respect to space and time, i.e. by applying the so-called Cauchy–Kovalewski procedure. However, this approach is not able to handle stiff source terms. Therefore, we present a new strategy that only replaces the Cauchy–Kovalewski procedure compared to the previously mentioned schemes. For the time-evolution part of the algorithm, we introduce a *local* space–time discontinuous Galerkin (DG) finite element scheme that is able to handle also stiff source terms. This step is the only part of the algorithm which is locally implicit. The third and last step of the proposed ADER finite volume schemes consists of the standard explicit space–time integration over each control volume, using the local space–time DG solutions at the Gaussian integration points for the intercell fluxes and for the space–time integral over the source term. We will show numerical convergence studies for nonlinear systems in one space dimension with both non-stiff and with very stiff source terms up to sixth order of accuracy in space and time. The application of the new method to a large set of different test cases is shown, in particular the stiff scalar model problem of LeVeque and Yee [R.J. LeVeque, H.C. Yee, A study of numerical methods for hyperbolic conservation laws with stiff source terms, Journal of Computational Physics 86 (1) (1990) 187–210], the relaxation system of Jin and Xin [S. Jin, Z. Xin, The relaxation schemes for systems of conservation laws in arbitrary space dimensions, Communications on Pure and Applied Mathematics 48 (1995) 235–277] and the full compressible Euler equations with stiff friction source terms.

Keywords: Hyperbolic balance laws; Stiff source terms; Finite volume schemes; ADER approach; Local space–time discontinuous Galerkin method; WENO reconstruction

* Corresponding author. Tel.: +49 170 9360238; fax: +49 711 68563438.
E-mail addresses: michael.dumbser@iag.uni-stuttgart.de (M. Dumbser), cedric.enaux@centraliens.net (C. Enaux), toro@ing.unitn.it (E.F. Toro).

0021-9991/$ - see front matter © 2007 Elsevier Inc. All rights reserved.
doi:10.1016/j.jcp.2007.12.005

1. Introduction

In this paper, we are concerned with solving numerically one-dimensional hyperbolic systems of *balance* laws (SBL), namely

$$\frac{\partial}{\partial t}\mathbf{u}+\frac{\partial}{\partial x}\mathbf{f}(\mathbf{u})=\mathbf{S}(\mathbf{u},x,t), \tag{1}$$

where $\mathbf{u}=\mathbf{u}(x,t)$ is the conservative state, $\mathbf{f}(\mathbf{u})$ is the flux and $\mathbf{S}(\mathbf{u},x,t)$ is the source term. The homogeneous system associated to (1) is the following hyperbolic system of conservation laws (SCL):

$$\frac{\partial}{\partial t}\mathbf{u}+\frac{\partial}{\partial x}\mathbf{f}(\mathbf{u})=0. \tag{2}$$

The definition of hyperbolicity only concerns system (2) above; it means that the Jacobian matrix of $\mathbf{f}(\mathbf{u})$ with respect to $\mathbf{u}$ has real eigenvalues and a set of associated eigenvectors which form a basis of $\mathbb{R}^d$, where d is the dimension of vector $\mathbf{u}$.

Coming from a wide range of different fields, a large number of physical models can be cast in the SBL form (1). Fluid mechanics is particularly concerned, since compressible fluid dynamics is usually modeled by the Euler system, which is a hyperbolic SCL. In this case, the source term can model the presence of other physical phenomena, such as gravity, reaction or friction.

We now restrict our analysis to source terms of the form $\mathbf{S}(\mathbf{u},x)$. Compared with SCL, the presence of a source term generally has important consequences on the behaviour of SBL solutions. First, SBL may have non-trivial *steady solutions*, namely solutions $\tilde{\mathbf{u}}(x)$ of the following system:

$$\frac{\partial}{\partial x}\mathbf{f}(\tilde{\mathbf{u}})=\mathbf{S}(\tilde{\mathbf{u}},x). \tag{3}$$

Second, SBL may tend towards reduced systems as we will explain now. At least two processes are involved in SBL: a conservative process associated to the homogeneous part (2) with a characteristic speed v_f, and a dissipative/productive process associated to the source term $\mathbf{S}$ with a characteristic speed v_S. If the time derivative is scaled according to the speed v_f, the dimensionless form of SBL (1) reads as

$$\frac{\partial}{\partial \bar{t}}\bar{\mathbf{u}}+\frac{\partial}{\partial \bar{x}}\bar{\mathbf{f}}(\bar{\mathbf{u}})=\frac{1}{\epsilon}\bar{\mathbf{S}}(\bar{\mathbf{u}},\bar{x}), \tag{4}$$

where bars mean that variables are dimensionless and where $\epsilon\equiv\frac{v_f}{v_S}$ is the ratio between characteristic speeds. A very small ratio $\epsilon\ll 1$ means that the dissipative/productive process is too fast, compared with the conservative process, to be fully observed. Such a source term is called *stiff* source term. The presence of a stiff source term may make tending the original system towards an asymptotic *reduced system* (see [12]), which can be of different mathematical nature than the original one. This situation occurs for instance in the case of an isentropic Euler system with large friction: the asymptotic limit of the original hyperbolic system is the porous media equation (see [30,31]), which is parabolic.

By integrating system (1) over a finite space–time control volume $\mathcal{Q}_i$ one obtains a finite volume formulation for the system of balance laws (1), which usually takes the form

$$\bar{\mathbf{u}}_i^{n+1}=\bar{\mathbf{u}}_i^{n}-\frac{\Delta t}{\Delta x_i}\left(\mathbf{f}_{i+\frac{1}{2}}-\mathbf{f}_{i-\frac{1}{2}}\right)+\Delta t\overline{\mathbf{S}}_i. \tag{5}$$

The integration of (1) in space and time gives rise to a temporal integral of the flux across the element boundaries $\mathbf{f}_{i+\frac{1}{2}}$ and to a space–time integral $\overline{\mathbf{S}}_i$ of the source term inside $\mathcal{Q}_i$. In practice, one must replace the integrals of the flux and the source in (5) by some suitable approximations, that is to say one must choose a concrete numerical scheme. For SCL, only a numerical flux must be chosen. In this case, the classical properties required are consistency, stability and accuracy. For SBL also a numerical source must be chosen. Here, not only the three classical properties are required, but some additional properties are needed for the global numerical scheme: It should be *well-balanced*, i.e. able to preserve steady states numerically. It should be robust also on *coarse grids* if the source term is stiff. A coarse grid is a grid whose size does not take into account the source term, i.e. the characteristic space and time steps are based on the associated homogeneous SCL only. Finally, the scheme should be *asymptotically consistent* or in other words *asymptotic preserving* if the

source term is stiff. This means that the scheme should give the correct asymptotic behaviour even if the source term is under resolved.

In the last three decades, powerful numerical fluxes have been proposed to solve hyperbolic SCL, for example the fluxes of Godunov [22], Osher [20,46] and Roe [54] as well as the various HLL-type fluxes based on the approximate Riemann solver of Harten et al. [28], see e.g. [18,19,63]. A naive approach to solve SBL would consist of using one of these schemes for the flux $\mathbf{f}_{i+\frac{1}{2}}$ and using a space-centered explicit scheme for the source $\overline{\mathbf{S}}_i$. However, treating the source explicitly may require prohibitively small time steps for stability reasons in the stiff case. In order to counter that, the numerical source is usually taken implicitly. However, it is well-known that using a classical numerical flux and a space-centered numerical source leads to spurious numerical results; more precisely, the global scheme is neither well-balanced, see for instance [3,26,24], nor asymptotically consistent, see e.g. [48,9,6]. Consequently, other approaches have been proposed to overcome that, as we will see in the following paragraph.

To solve SBL, very commonly used approaches are *splitting* schemes. A splitting approach (also called *fractional step method*) consists of solving iteratively the associated SCL with a classical finite volume scheme, and then the system of ODE associated to the source term with a classical numerical tool, like Runge–Kutta or predictor–corrector methods. The accuracy of the global scheme depends on the number and the order of these sub-steps; for example, a three sub-stage Strang splitting (see [57]) is second-order accurate in time, but in the non-stiff case only, as pointed out in [33]. Although simple and robust, classical first-order splittings and Strang splittings lead to global schemes that are neither well-balanced, nor asymptotically consistent (see [41]) because the coupling between numerical flux and numerical source only occurs through the initial condition of each sub-step. Better splitting schemes for particular SBL have been proposed (see [1,9,44,10]), and are asymptotically consistent because at least one of the sub-steps takes into account both flux divergence and source term. The high-order splitting scheme proposed by Pareschi and Russo [47] is asymptotically consistent with the stiff limit and can also reach high order of accuracy in the stiff limit, but it is not uniformly accurate in the whole possible range of the stiffness parameter ϵ.

Another approach to solve SBL consists of upwinding the source at the interfaces (*USI schemes*). In the original version of USI schemes (see [3,35]), a classical Riemann solver is first used to evaluate numerically the solution $\mathbf{u}_{i+\frac{1}{2}}$ of the homogeneous Riemann problem (without source term). This solution is then used in a first-order finite volume scheme as argument of the flux, but also as argument of the source term in $\overline{\mathbf{S}}_i = \frac{1}{2}\left(\mathbf{S}\left(\mathbf{u}_{i-\frac{1}{2}}\right) + \mathbf{S}\left(\mathbf{u}_{i+\frac{1}{2}}\right)\right)$, so that the same numerical information – based on the homogeneous system only – is given to the flux and the source term, which makes the scheme at least approximately well-balanced. More recently, other USI scheme versions have been proposed, which ensure that the scheme is also formally well-balanced (see [50,4]). The main drawback of these approaches is that the global scheme must be explicit, thus problems may occur in the stiff case. In [6], a new version of USI schemes, designed for stiff relaxation SBL, has been proposed. The resulting scheme is robust, formally asymptotically consistent and stable under a classical CFL condition, but obtains only first order of accuracy.

In some of the *well-balanced schemes* proposed in the literature (for a non-exhaustive overview see [5,11,24,26,39]), the source term is seen as a nonconservative product of a larger system. Due to the presence of this nonconservative product, a particular path has to be chosen instead of the classical Rankine–Hugoniot relations. This path can be chosen in such a way that the well-balanced property is formally imposed to the scheme. Well-balanced schemes are very efficient to maintain steady states under classical CFL condition $\Delta t \simeq \mathcal{O}(\Delta x)$ (see [24]), but are not designed to capture the good asymptotic behaviour imposed by a stiff source term. More recently, a new version of well-balanced schemes which is also asymptotically consistent has been proposed for a particular system (see [25]), but the resulting scheme is only stable under a very restrictive parabolic CFL condition of the type $\Delta t \simeq \mathcal{O}(\Delta x^2)$.

To solve SBL numerically, other approaches have been proposed. Sometimes, the Riemann problem considered takes into account the presence of the source term (*generalized Riemann problem*), see [21,38,64]. However, these methods are not robust enough to deal with stiff source terms. Concerning stiff relaxation systems, another approach consists of solving numerically the asymptotic reduced system instead of solving the original SBL, see [2,6]. In this case, numerical results can only be obtained in the stiff case, thus some information is lost from the original SBL. In [43] it was pointed out that a semi-discrete discontinuous Galerkin (DG)

scheme, i.e. only applying the DG space-discretization and remaining continuous in time, is an asymptotically consistent scheme for linear systems with stiff relaxation. However, since the main problem of stiff SBL is precisely the *time discretization*, this theoretical result given in [43] is only of very limited use in practice. Another idea proposed in [8] to solve nonlinear SBL is to use a combination of two tools. First, a relaxation scheme (see [37]) is used in order to obtain a linear, but larger, SBL. Second, a well-balanced scheme designed to capture the good asymptotic behaviour is applied on the larger system. The global scheme has many good properties, but is only of first order of accuracy. Finally, some asymptotically consistent schemes have been derived using an upwind flux that has been modified by the presence of the source term, see [49,36,45].

To our knowledge, a lot of tools to solve numerically SBL have been proposed up to now. The best ones among those are well-balanced and asymptotically consistent, but none of them allows to reach very high orders of accuracy in space and time (greater than three) while being stable under classical CFL condition. The aim of this article is now to construct a numerical method for SBL that has a good asymptotic limit behaviour when the source terms are stiff and that can reach *any* order of accuracy in space and time under a standard CFL stability condition.

The structure of the paper is as follows: In Section 2, we show the construction of the proposed finite volume scheme. To assure monotonicity of the numerical solution in the vicinity of discontinuities, we briefly discuss the nonlinear WENO reconstruction operator in Section 2.1, which is necessary to obtain a high-order polynomial data representation from the given cell averages. In Section 2.2, a new local space–time discontinuous Galerkin scheme is introduced to evolve this polynomial data in time. Numerical convergence studies are then carried out in Section 3 and applications to various linear and nonlinear SBL with stiff source terms are shown in Section 4. A summary with conclusions and an outlook regarding future work is given in Section 5.

2. An explicit arbitrary high-order accurate finite volume scheme for nonlinear hyperbolic systems with stiff source terms

We consider hyperbolic systems of balance laws for the vector of conserved quantities $\mathbf{u} = \mathbf{u}(x,t)$ of the form

$$\begin{cases} \text{PDE}: & \frac{\partial}{\partial t}\mathbf{u} + \frac{\partial}{\partial x}\mathbf{f}(\mathbf{u}) = \mathbf{S}(\mathbf{u}), \\ \text{IC}: & \mathbf{u}(x,0) = \mathbf{u}_0(x), \end{cases} \tag{6}$$

where $\mathbf{f}(\mathbf{u})$ is in general a nonlinear function of the state $\mathbf{u}$ and $\mathbf{S}(\mathbf{u})$ may be a stiff nonlinear source term. To illustrate the general framework of the method in the simplest possible way we restrict ourselves in the whole paper to one space dimension. The extension to multiple space dimensions can be done and will be the topic of future research.

The spatial computational domain $\Omega \subset \mathbb{R}$ is covered completely by pairwise disjoint spatial elements $Q_i =]x_{i-\frac{1}{2}}; x_{i+\frac{1}{2}}[$, with $\Delta x_i = x_{i+\frac{1}{2}} - x_{i-\frac{1}{2}}$ and the cell average of $\mathbf{u}(x,t)$ within Q_i is defined at time t^n as

$$\bar{\mathbf{u}}_i^n = \frac{1}{\Delta x_i}\int_{x_{i-\frac{1}{2}}}^{x_{i+\frac{1}{2}}} \mathbf{u}(x,t^n)\mathrm{d}x. \tag{7}$$

We furthermore define the space–time element spanned by the spatial element Q_i and the time step $\Delta t = t^{n+1} - t^n$ as $\mathcal{Q}_i = Q_i \times]t^n; t^n + \Delta t[$. The associated relative space and time coordinates $0 \leqslant \xi \leqslant 1$ and $0 \leqslant \tau \leqslant 1$, within one element $\mathcal{Q}_i$ are given by the relations

$$x = x_{i-\frac{1}{2}} + \xi \cdot \Delta x_i, \quad \text{and} \quad t = t^n + \tau \cdot \Delta t. \tag{8}$$

In the following, the numerical solution of (6) valid inside each element $\mathcal{Q}_i$ will be denoted with $\mathbf{u}_i(\xi,\tau)$. A standard finite volume discretization of (6) is given after integration of (6) over each space–time element $\mathcal{Q}_i$ as follows:

$$\bar{\mathbf{u}}_i^{n+1} = \bar{\mathbf{u}}_i^n - \frac{\Delta t}{\Delta x_i}\left(\mathbf{f}_{i+\frac{1}{2}} - \mathbf{f}_{i-\frac{1}{2}}\right) + \Delta t \overline{\mathbf{S}}_i \tag{9}$$

with

$$\mathbf{f}_{i+\frac{1}{2}} = \int_0^1 \mathbf{f}_h(\mathbf{u}_i(1,\tau), \mathbf{u}_{i+1}(0,\tau))\mathrm{d}\tau \quad \text{and} \quad \overline{\mathbf{S}}_i = \int_0^1\int_0^1 \mathbf{S}(\mathbf{u}_i(\xi,\tau))\mathrm{d}\xi\,\mathrm{d}\tau, \tag{10}$$

where $\mathbf{f}_h(\mathbf{u}_i(1,\tau),\mathbf{u}_{i+1}(0,\tau))$ denotes a numerical flux function (Riemann solver) that depends on the two arguments $\mathbf{u}_i(1,\tau)$ and $\mathbf{u}_{i+1}(0,\tau)$, which are the boundary extrapolated data on the left and on the right side of the element interface $i+\frac{1}{2}$. For an overview of Riemann solvers see [61]. For all computations shown in this paper we use the Rusanov flux, which is also often called the local Lax–Friedrichs flux. The Rusanov flux is a special case of the HLL flux, with a particularly simple wave speed estimate which is taken to be the maximum of the absolute values of the left and right eigenvalues. For an explicit standard first-order Godunov-type finite volume scheme, one would now simply have to set $\mathbf{u}_i(\xi,\tau)=\bar{\mathbf{u}}_i^n$ and $\mathbf{u}_{i+1}(\xi,\tau)=\bar{\mathbf{u}}_{i+1}^n$ for the arguments of the numerical flux and inside the source term integral.

We emphasize that formula (9) together with (10) allows the construction of *arbitrary* high-order accurate finite volume schemes, provided the representation of the numerical solution $\mathbf{u}_i(\xi,\tau)$ inside each element and as a consequence the arguments of the numerical flux function and the source term are high-order accurate in space and time. Since (9) only computes the time update of the cell averages $\bar{\mathbf{u}}_i^n$ from time t^n to time t^{n+1} we need to reconstruct higher-order polynomial data from these cell averages $\bar{\mathbf{u}}^n$ to get better estimates for the arguments of the flux function and the source term in the integrals appearing in (10).

Therefore, as described in detail in the subsequent sections, the necessary steps to construct an arbitrary high-order essentially non-oscillatory explicit one-step finite volume scheme are the following: (I) Nonlinear (non-oscillatory) reconstruction of spatial polynomials from the given cell averages at time t^n. (II) Local solution of the initial value problem (6) inside each element, where the initial data is given by the spatial reconstruction polynomial at time t^n. (III) Numerical integration of the integrals in (10) and update of the cell averages according to (9).

2.1. Nonlinear reconstruction technique

In this section, we briefly discuss the proposed nonlinear weighted essentially non-oscillatory (WENO) reconstruction procedure to reconstruct higher-order polynomial data within each spatial cell Q_i at time t^n from the given cell averages $\bar{\mathbf{u}}_i^n$. This corresponds to step (I) as outlined at the end of the previous section. We emphasize already at this point that the reconstruction procedure is *nonlinear* and depends strongly on the input data $\bar{\mathbf{u}}_i^n$. Thus, the resulting numerical scheme, even when applied to a completely linear PDE, will be *nonlinear* and thus it will not be possible to give a closed expression of the scheme.

The reconstruction procedure described here for the one-dimensional case follows directly from the guidelines given in [14] for general unstructured two- and three-dimensional meshes. It reconstructs *entire polynomials*, as the original ENO approach proposed by Harten et al. in [27]. However, we formally write our method like a WENO scheme [32,42] with a particularly simple choice for the linear weights. The most important difference of our approach compared to classical WENO schemes is that standard WENO methods reconstruct *point values* at the Gaussian integration points instead of an entire polynomial valid inside each element Q_i.

Reconstruction is done for each element on a reconstruction stencil $\mathcal{S}_i^s$, which is given by the following union of the element Q_i and its neighbors Q_j:

$$\mathcal{S}_i^s=\bigcup_{j=i+s-k}^{i+s+k} Q_j, \tag{11}$$

where s is the stencil shift with respect to the central element Q_i and k is the spatial extension of the stencil to the left and the right. A central reconstruction stencil is given by $s=0$, an entirely left-sided stencil is given by $s=-k$ and an entirely right-sided stencil is given by $s=k$. In our approach, we always will use the three fixed reconstruction stencils $\mathcal{S}_i^0$, $\mathcal{S}_i^{-k}$ and $\mathcal{S}_i^k$.

Given the cell average data $\bar{\mathbf{u}}_i^n$ in all elements Q_i we are looking for a spatial reconstruction polynomial obtained from $\mathcal{S}_i^s$ at time t^n of the form:

$$\mathbf{w}_i^s(\xi,t^n)=\sum_{l=0}^{M}\Psi_l(\xi)\hat{\mathbf{w}}_l^{(i,s)}(t^n):=\Psi_l(\xi)\hat{\mathbf{w}}_l^{(i,s)}(t^n), \tag{12}$$

where we use the rescaled Legendre polynomials for the spatial reconstruction basis functions $\Psi_l(\xi)$ such that the $\Psi_l(\xi)$ form an orthogonal basis on the unit interval $I = [0;1]$. In the following, we will use standard tensor index notation, implying summation over indices appearing twice. The number of polynomial coefficients (degrees of freedom) is $L = M + 1$, where M is the degree of the reconstruction polynomial. To compute the reconstruction polynomial $\mathbf{w}_i(\xi, t^n)$ valid for element Q_i we require integral conservation for all elements Q_j inside the stencil $\mathcal{S}_i^s$, i.e.

$$\int_{Q_j} \mathbf{w}_i^s(\xi, t^n)\mathrm{d}\xi = \int_{Q_j} \Psi_l(\xi)\mathrm{d}\xi \cdot \hat{\mathbf{w}}_l^{(i,s)}(t^n) = \bar{\mathbf{u}}_j^n \quad \forall Q_j \in \mathcal{S}_i^s. \tag{13}$$

Eq. (13) yields a linear equation system of the form

$$A_{jl} \cdot \hat{\mathbf{w}}_l^{(i,s)}(t^n) = \bar{\mathbf{u}}_j^n \tag{14}$$

for the unknown coefficients $\hat{\mathbf{w}}_l^{(i,s)}(t^n)$ of the reconstruction polynomial on stencil $\mathcal{S}_i^s$. Since we choose $k = M/2$ for even M and $k = (M+1)/2$ for odd M, the number of elements in $\mathcal{S}_i^s$ may become larger than the number of degrees of freedom L. In this case, we use a constrained least-squares technique according to [14] to solve (14).

To obtain the final non-oscillatory reconstruction polynomials for each Q_i at time t^n, we finally construct a data-dependent nonlinear combination of the polynomials $\mathbf{w}_i^0(\xi, t^n)$, $\mathbf{w}_i^{-k}(\xi, t^n)$ and $\mathbf{w}_i^k(\xi, t^n)$ obtained from the central, left-sided and right-sided stencils as follows:

$$\mathbf{w}_i(\xi, t^n) = \hat{\mathbf{w}}_l^i(t^n)\Psi_l(\xi) \tag{15}$$

with

$$\hat{\mathbf{w}}_l^i(t^n) = \omega_0 \hat{\mathbf{w}}_l^{(i,0)}(t^n) + \omega_{-k}\hat{\mathbf{w}}_l^{(i,-k)}(t^n) + \omega_k \hat{\mathbf{w}}_l^{(i,k)}(t^n). \tag{16}$$

The nonlinear weights ω_s are given by the relations

$$\omega_s = \frac{\tilde{\omega}_s}{\tilde{\omega}_0 + \tilde{\omega}_{-k} + \tilde{\omega}_k}, \quad \tilde{\omega}_s = \frac{\lambda_s}{(\sigma_s + \epsilon)^r}. \tag{17}$$

In our particular formulation, the oscillation indicators σ_s are computed from

$$\sigma_s = \Sigma_{lm}\hat{\mathbf{w}}_l^s(t^n)\hat{\mathbf{w}}_m^s(t^n) \quad \text{with } \Sigma_{lm} = \sum_{\alpha=1}^{M} \int_0^1 \frac{\partial^\alpha \Psi_l(\xi)}{\partial \xi^\alpha} \cdot \frac{\partial^\alpha \Psi_m(\xi)}{\partial \xi^\alpha} \mathrm{d}\xi. \tag{18}$$

Here, Σ_{lm} is the universal oscillation indicator matrix for the reference element Q_E that does neither depend on the problem nor on the mesh, see [14]. The parameters ϵ and r are constants for which we typically choose $\epsilon = 10^{-14}$ and $r = 12$. For the linear weights λ_s we choose $\lambda_{-k} = \lambda_k = 1$ and a very large linear weight λ_0 on the central stencil, typically $\lambda_0 = 10^5$. It has been shown previously [32,42] that the numerical results are quite insensitive to the WENO parameters ϵ and r and also with respect to the linear weight on the central stencil λ_0, see [14].

The proposed reconstruction usually uses the accurate and linearly stable central stencil reconstruction in those regions of Ω where the solution is smooth because of the large linear weight λ_0. However, due to the strongly nonlinear dependence of the weights ω_s on the oscillation indicators σ_s, in the presence of discontinuities the smoother left- or right-sided stencils are preferred, as for standard ENO and WENO methods. For the nonlinear scalar case, the reconstruction operator described above can be directly applied to the cell averages $\bar{u}_i^n$ of the conserved quantity u. For nonlinear hyperbolic systems, the reconstruction should be done in characteristic variables [27,15] in order to avoid spurious oscillations that may appear when applying ENO or WENO reconstruction operators component-wise to nonlinear hyperbolic systems.

The result of the reconstruction procedure is a non-oscillatory spatial polynomial $\mathbf{w}_i(\xi, t^n)$ defined at time t^n inside each spatial element Q_i. However, we still need to compute the temporal evolution of these polynomials inside each space–time element $\mathcal{Q}_i$ in order to be able to compute the integrals appearing in (10).

2.2. The local space–time discontinuous Galerkin scheme

In previously published ADER finite volume schemes (see e.g. [14,15,60,65]) and also in the original ENO scheme of Harten et al. [27] the nonlinear reconstruction step (I) as well as the numerical integration and update step (III) as outlined at the end of Section 2 are very similar compared with the new scheme proposed in this article. The only main difference lies in the solution of the local initial value problem (IVP) defined in step (II). In ADER finite volume schemes and also in the original ENO approach the temporal evolution of the reconstruction polynomial is computed using the so-called Cauchy–Kovalewski or Lax–Wendroff procedure. This procedure constructs a local solution of the IVP making the ansatz of a local time Taylor series expanded at time level t^n, where then time derivatives are replaced by spatial derivatives differentiating repeatedly the governing PDE with respect to space and time. The spatial derivatives are obtained from the reconstruction polynomials at time t^n. In [17,55] it has been shown analytically via differential approximation and also numerically that these finite volume schemes can reach any order of accuracy in space and time.

It is a well-known fact that methods based on Taylor series usually do not work in the presence of stiff source terms. Therefore, we propose to replace the Cauchy–Kovalewski procedure by a new local space–time DG scheme in order to solve the local IVP in step (II). In our local space–time DG scheme, the usual integration by parts is done only in time and not in space, which establishes a distinct difference compared to the existing global space–time DG schemes [66]. A comparison of the classical Cauchy–Kovalewski procedure and the new local space–time DG scheme will be shown for a simple case to illustrate the difference in the quality of the solution of the local IVP.

2.2.1. Linear scalar model equation

To illustrate the construction and the theoretical properties of our proposed method, in this section we only consider the simple linear scalar model equation with the linear flux and source functions:

$$f(u) = au \quad \text{and} \quad S(u) = -vu, \qquad a > 0, \;\; v > 0, \tag{19}$$

where the stiffness of the relaxation source term is determined by the parameter v and where we suppose periodic boundary conditions for the moment.

The space of basis and test functions V_h of the local space–time DG scheme is defined to be the space spanned by piecewise polynomials given by the space–time tensor products of the scaled Legendre polynomials $\Psi_i(\xi)$ and $\Psi_j(\tau)$ of degree $0 \leqslant i, j \leqslant M$, i.e.

$$\Phi_k = \Phi_k(\xi,\tau) = \Psi_i(\xi) \cdot \Psi_j(\tau). \tag{20}$$

In Eq. (20) the index k with $1 \leqslant k = k(i,j) \leqslant N_d$ is a mono-index ranging from 1 to the number of degrees of freedom $N_d = (M+1)^2$, computed from the index pair (i,j). As already defined above, $0 \leqslant \xi \leqslant 1$ and $0 \leqslant \tau \leqslant 1$ are the spatial and the temporal coordinates in the space–time reference element $\mathcal{Q}_E = [0;1] \times [0;1] \in \mathbb{R}^2$. In the following, we will use the following two scalar products of two functions $f(\xi,\tau)$ and $g(\xi,\tau)$:

$$\langle f, g \rangle = \int_0^1 \int_0^1 f(\xi,\tau) \cdot g(\xi,\tau) \mathrm{d}\xi \, \mathrm{d}\tau, \quad [f,g]_\tau = \int_0^1 f(\xi,\tau) \cdot g(\xi,\tau) \mathrm{d}\xi, \tag{21}$$

where the first one denotes the space–time scalar product over the space–time reference element $\mathcal{Q}_E$ and the second one is the purely spatial scalar product over the spatial reference element $Q_E = [0;1]$ at time τ. The local numerical solution u_i of (6) inside each space–time control volume $\mathcal{Q}_i$ is approximated within the reference element $\mathcal{Q}_E$ using the basis functions Φ_k as follows:

$$u_i = u_i(\xi,\tau) = \sum_{l=1}^{N^d} \Phi_l(\xi,\tau) \cdot \hat{u}_l^i := \Phi_l(\xi,\tau) \hat{u}_l^i, \tag{22}$$

where we again use the classical Einstein summation convention for tensor calculus, which implies summation over all indices appearing twice.

The proposed local space–time discontinuous Galerkin finite element method is now obtained by first rewriting the governing PDE (6) together with the assumption (19) in terms of the variables in the reference element, i.e.

$$\frac{\partial}{\partial\tau}u + a^*\frac{\partial}{\partial\xi}u = -v^*u \tag{23}$$

with $a^* = \Delta t\xi_x \cdot a$ and $v^* = \Delta t \cdot v$.

Multiplication of the modified governing PDE with test functions $\Phi_k \in V_h$ and integration over the reference element $\mathcal{Q}_E$ yields

$$\left\langle \Phi_k, \frac{\partial}{\partial\tau}u_i \right\rangle + a^*\left\langle \Phi_k, \frac{\partial}{\partial\xi}u_i \right\rangle = -v^*\langle \Phi_k, u_i\rangle. \tag{24}$$

For the space–time discontinuous Galerkin scheme presented in [66] one would now have to integrate both terms on the left-hand side by parts in space and time in order to introduce the information from the neighbor elements and to shift the spatial derivative operator onto the test function. For our purposes, however, the integration by parts in space is *not* required since we want to keep a *local* formulation that does not need any information from the neighbor elements but for which it is sufficient to provide an initial condition. Therefore, we only use the integration by parts in time for the first term that contains the time derivative, and obtain

$$[\Phi_k, u_i]_1 - [\Phi_k, w_i]_0 - \left\langle \frac{\partial}{\partial\tau}\Phi_k, u_i \right\rangle + a^*\left\langle \Phi_k, \frac{\partial}{\partial\xi}u_i \right\rangle = -v^*\langle \Phi_k, u_i\rangle. \tag{25}$$

The spatial scalar products appearing in (25) correspond to the fluxes in time direction. Due to the causality principle the future has no influence on the past, i.e. we can take the numerical solution *inside* the element itself for the flux at relative time $\tau = 1$, whereas the flux at relative time $\tau = 0$ will be completely defined by the initial condition $w_i = w_i(\xi, t^n) = \Psi_m(\xi)\hat{w}_m^i(t^n)$. The initial condition is hence given by the reconstruction polynomials obtained from the reconstruction operator applied to the cell averages at the current time t^n. We recall that the $\Psi_m(\xi)$ are the reconstruction basis functions introduced in Section 2.1. Please note that due to the use of a *discontinuous* Galerkin approximation, in general $w_i(\xi, t^n) \neq u_i(\xi, 0^+)$, i.e. the reconstruction polynomials at $t = t^n$ do not necessarily agree with the boundary extrapolated polynomial $u_i(\xi, 0^+)$ of the space–time DG solution inside element $\mathcal{Q}_i$ at $\tau = 0^+$. Inserting the time fluxes and the ansatz for the numerical solution (22) into (25) yields

$$\left([\Phi_k, \Phi_l]_1 - \left\langle \frac{\partial}{\partial\tau}\Phi_k, \Phi_l \right\rangle + a^*\left\langle \Phi_k, \frac{\partial}{\partial\xi}\Phi_l \right\rangle + v^*\langle \Phi_k, \Phi_l\rangle\right)\hat{u}_l^i = [\Phi_k, \Psi_m]_0\hat{w}_m^i(t^n). \tag{26}$$

Introducing the element mass matrix $M_{kl} = \langle \Phi_k, \Phi_l\rangle$, the stiffness matrices with respect to time $K_{kl}^\tau = \left\langle \frac{\partial}{\partial\tau}\Phi_k, \Phi_l \right\rangle$ and space $K_{kl}^\xi = \left\langle \Phi_k, \frac{\partial}{\partial\xi}\Phi_l \right\rangle$ as well as the flux matrices $F_{km}^0 = [\Phi_k, \Psi_m]_0$ and $F_{kl}^1 = [\Phi_k, \Phi_l]_1$ for time $\tau = 0$ and $\tau = 1$, we obtain the following equation system for the unknowns $\hat{u}_l^i$:

$$Y_{kl}\hat{u}_l^i = F_{km}^0\hat{w}_m^i(t^n). \tag{27}$$

The system has a unique solution if the system matrix

$$Y_{kl} = F_{kl}^1 - K_{kl}^\tau + a^*K_{kl}^\xi + v^*M_{kl} \tag{28}$$

is invertible. It will be shown in the following that this is always the case for any value of v. Therefore, the solution of (27) can be written as

$$\hat{u}_l^i = Y_{kl}^{-1} \cdot F_{km}^0\hat{w}_m^i(t^n). \tag{29}$$

We note that the local space–time DG scheme (26) requires the solution of the linear equation system (27) and thus is *locally implicit*. Due to the local character of the method, the computation of the space–time degrees of freedom $\hat{u}_l^i$ can be done independently for each cell $\mathcal{Q}_i$, without considering neighbor elements. However, we emphasize that this is the only locally implicit part of the entire algorithm. The resulting finite volume scheme (9) is completely explicit.

2.2.2. Properties of the local space–time discontinuous Galerkin scheme

2.2.2.1. Well-posedness. The mass matrix M_{kl} is diagonal since the functions $\Phi_k(\xi,\tau)$ form an orthogonal basis on the space–time reference element $\mathcal{Q}_E$ with respect to the scalar product $\langle\cdot,\cdot\rangle$. Therefore, the system matrix Y_{kl} is diagonally dominant in the case $v \to \infty$ and thus system (27) will be always well posed, especially in the stiff limit.

2.2.2.2. Boundedness of the solution. In the following we want to show via asymptotic analysis that the solution u_i of (26) remains bounded in the limit $v \to \infty$. Even more, we will show that the discrete solution of (26) tends to zero as $v \to \infty$. We therefore write (26) with $\Phi_k \in V_h$ and $v^* = 1/\epsilon$, where $\epsilon > 0$ is a small parameter and $v \to \infty$ for $\epsilon \to 0$, as follows:

$$[\Phi_k, u_i]_1 - [\Phi_k, w_i]_0 - \left\langle \frac{\partial}{\partial\tau}\Phi_k, u_i \right\rangle + a^* \left\langle \Phi_k, \frac{\partial}{\partial\xi} u_i \right\rangle = -\frac{1}{\epsilon}\langle \Phi_k, u_i\rangle. \tag{30}$$

Furthermore, we write a series expansion for $u_i = u_i(\xi,\tau)$ in terms of the small parameter ϵ with $u_0 \in V_h$, $u_1 \in V_h$, and $u_2 \in V_h$ as

$$u_i = u_0 + \epsilon^1 u_1 + \epsilon^2 u_2 + \mathcal{O}(\epsilon^3). \tag{31}$$

After inserting (31) into (30) we obtain the following equation system retaining only terms up to power ϵ^1:

$$[\Phi_k, u_0 + \epsilon u_1]_1 - [\Phi_k, w_i]_0 - \left\langle \frac{\partial}{\partial\tau}\Phi_k, u_0 + \epsilon u_1 \right\rangle + a^* \left\langle \Phi_k, \frac{\partial}{\partial\xi}(u_0 + \epsilon u_1) \right\rangle = -\frac{1}{\epsilon}\langle \Phi_k, u_0 + \epsilon u_1 + \epsilon^2 u_2\rangle. \tag{32}$$

Since Eq. (32) must be fulfilled for *any* value of $\epsilon > 0$, all coefficients after the terms in ϵ must vanish. From the leading term ϵ^{-1} we therefore obtain

$$\langle \Phi_k, u_0\rangle = 0 \quad \forall \Phi_k \in V_h \quad \Rightarrow \quad u_0 = 0. \tag{33}$$

Inserting (33) in (32) and considering the coefficients of the terms ϵ^0 we obtain

$$\langle \Phi_k, u_1\rangle - [\Phi_k, w_i]_0 = 0 \tag{34}$$

and from the term ϵ^1 we get

$$\langle \Phi_k, u_2\rangle - \left\langle \frac{\partial}{\partial\tau}\Phi_k, u_1 \right\rangle + a^* \left\langle \Phi_k, \frac{\partial}{\partial\xi} u_1 \right\rangle = 0. \tag{35}$$

Eqs. (34) and (35) connect u_1 and u_2 with the initial condition $w_i(\xi, t^n)$. Since $w_i(\xi, t^n)$ does not depend explicitly on ϵ, from Eqs. (33)–(35) and the ansatz (31) follows:

$$\lim_{\epsilon\to 0} u_i(\xi,\tau) = \lim_{\epsilon\to 0}(\epsilon u_1 + \epsilon^2 u_2 + \mathcal{O}(\epsilon^3)) = 0. \tag{36}$$

From (36) follows the boundedness of $u_i(\xi,\tau)$ in $\mathcal{Q}_i$ in the stiff limit $\epsilon \to 0$. This property is necessary to eliminate the stiffness from the numerical flux in (10) in the limit $\epsilon \to 0$. For our model problem (19) the numerical flux $f_h(u_i(1,\tau), u_{i+1}(0,\tau))$ in (10) is a *linear* function of its two arguments $u_i(1,\tau)$ and $u_{i+1}(0,\tau)$. Since (36) is valid independently for all elements $\mathcal{Q}_i$, we get $f_{i+\frac{1}{2}} \to 0$ and $f_{i-\frac{1}{2}} \to 0$ for $\epsilon \to 0$.

2.2.2.3. Boundedness of the source term integral. Even more important for the robustness of the finite volume scheme (9) is the boundedness of the source space–time integral $\overline{S}_i$ defined in (10). For the linear scalar model Eq. (19) the source space–time integral reads with $1/\epsilon = v^* = \Delta t v$ together with the asymptotic ansatz (31) and Eq. (33) as

$$\overline{S}_i = -v\langle 1, u_i\rangle = -\Delta t^{-1}\frac{1}{\epsilon}\langle 1, u_i\rangle = -\frac{1}{\Delta t}\langle 1, u_1 + \epsilon^1 u_2 + \mathcal{O}(\epsilon^2)\rangle. \tag{37}$$

Using (34) and the conservation property (13) of the reconstruction operator, i.e. $[1, w_i]_0 = \bar{u}_i^n$, we finally obtain

$$\overline{S}_i = -\frac{1}{\Delta t}([1, w_i]_0 + \mathcal{O}(\epsilon)) = -\frac{1}{\Delta t}(\bar{u}_i^n + \mathcal{O}(\epsilon)) \tag{38}$$

and in the stiff limit $\epsilon \to 0$ we have

$$\lim_{\epsilon \to 0} \overline{S}_i = -\frac{\bar{u}_i^n}{\Delta t}. \tag{39}$$

Inserting (36) and (39) into (9) and (10), we obtain the following finite volume scheme in the stiff limit:

$$\lim_{\epsilon \to 0} \bar{u}_i^{n+1} = \bar{u}_i^n + \frac{\Delta t}{\Delta x} \lim_{\epsilon \to 0} \left(f_{i+\frac{1}{2}} - f_{i-\frac{1}{2}} \right) + \Delta t \lim_{\epsilon \to 0} \overline{S}_i = 0. \tag{40}$$

This means that for *any* bounded initial condition $\bar{u}_i^n$ and for any bounded Δt (e.g. bounded by the standard CFL condition) our finite volume scheme of any order of accuracy captures the stiff limit of (6) with (19).

2.2.2.4. Asymptotic preserving (AP) property. In Appendix C, we show that the local space–time DG scheme has the AP property in the sense of [34] for a simple linear model system at least for polynomial approximation spaces of degree greater or equal two.

2.2.3. Comparison of the Cauchy–Kovalewski procedure with the local space–time DG scheme for a linear scalar ODE

As mentioned already before, in the original ENO approach of Harten et al. [27] and also for ADER finite volume and discontinuous Galerkin schemes [14,15,13,16,60,62], the time-accurate temporal evolution of the reconstruction polynomials $w_i(\xi, t^n)$ is predicted inside each element within one time step using the Cauchy–Kovalewski procedure, where the local solution is computed via a temporal Taylor series in which the time derivatives are replaced by space derivatives using repeated differentiation of the governing partial differential equation (6). As an initial condition for this procedure, the reconstruction polynomials $w_i(\xi, t^n)$ at time $t = t^n$ are taken. In other words, we are looking for a *local* solution $u_i(\xi, \tau)$ of the initial value problem for (6) *inside* each space–time element $\mathcal{Q}_i$, where the initial condition is given by the reconstruction polynomials, i.e. $u(x(\xi), 0) = w_i(\xi, t^n)$.

Neglecting convection for the moment, i.e. setting $a = 0$, the PDE (6) with (19) reduces to the simple linear ordinary differential equation

$$\frac{\partial}{\partial t} u = -\nu u, \quad t \in \mathbb{R}_0^+, \tag{41}$$

whose solution is given by

$$u(t, \nu) = u(0) \mathrm{e}^{-\nu t}. \tag{42}$$

For very large values of ν, the solution (42) tends to the discontinuous limit solution

$$\lim_{\nu \to \infty} u(t, \nu) = \begin{cases} u(0) & \text{if } t = 0, \\ 0 & \text{if } t > 0. \end{cases} \tag{43}$$

It is obvious that a Taylor series expanded at time $t = 0$ is not able to approximate such a discontinuous solution as given by (43). For this reason, the Cauchy–Kovalewski method cannot be applied in this case to construct a local solution to (6) since it is based essentially on the applicability of the Taylor series expansion in time. In order to construct a polynomial approximation to (42) that is at the same time high-order accurate *and* is able to capture the stiff limit (43), we have proposed the new local space–time discontinuous Galerkin scheme (27) applied to (6) locally inside each element. The solution $u_i(\xi, \tau)$ of this local space–time DG scheme applied to all elements $\mathcal{Q}_i$ is used in the finite volume scheme (9) to compute the numerical fluxes at the element interfaces and to compute the space–time integral of the source term in (10).

In Fig. 1 we show the numerical solutions obtained with sixth-order schemes (basis polynomials Φ_k of maximal degree five) applied to (41) for increasing values of ν with the initial condition $u(0) = 1$. This figure shows very clearly that the Cauchy–Kovalewski procedure already fails for the small value of $\nu = 3$. For very large values of ν, the solution of the Cauchy–Kovalewski procedure is only correct in a very small interval $[0; \delta]$ $(0 < \delta \ll 1)$ and diverges quickly in the remaining interval $]\delta; 1]$, whereas our new local space–time DG scheme apparently converges to the correct solution (43) of (41) for $\nu \to \infty$ in the interval $]\delta; 1]$. We note fur-

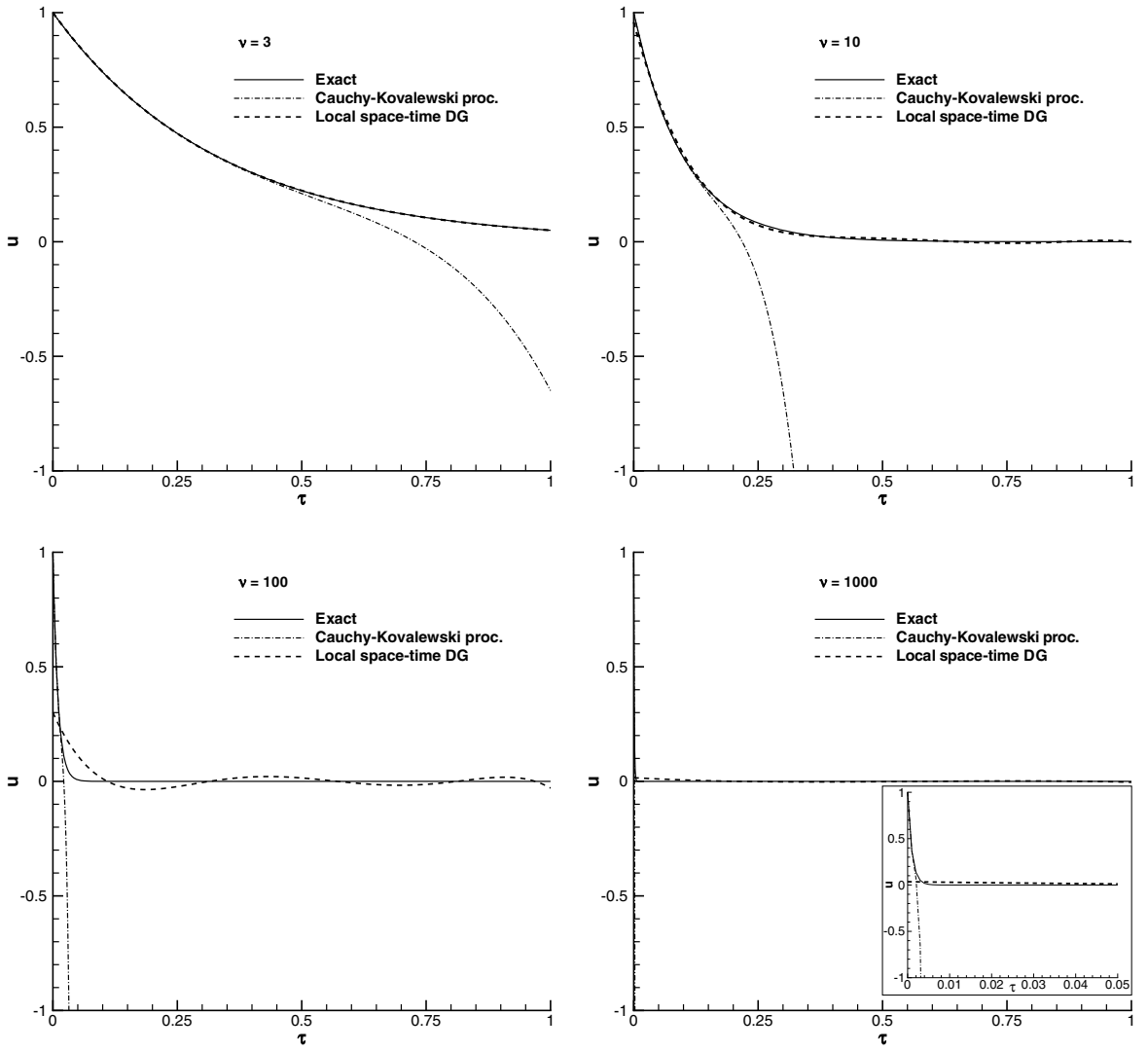

Fig. 1. Exact solution and sixth-order numerical solutions of (41) using the Cauchy–Kovalewski procedure based on a temporal Taylor series expansion and the new local space–time DG scheme for $v = 3$ (top left), $v = 10$, (top right), $v = 100$ (bottom left) and $v = 1000$ (bottom right).

thermore that the local space–time DG scheme produces an almost continuous solution at $\tau = 0$ for small values of v and exhibits an increasing jump at $\tau = 0$ for increasing v in order to capture correctly the discontinuous behaviour of (42). Note that in all cases shown $u(0) = 1$.

2.2.4. General linear hyperbolic systems with stiff source terms

The extension of the proposed local space–time discontinuous Galerkin scheme to general linear hyperbolic systems is straightforward. We consider linear systems of the form:

$$\frac{\partial}{\partial t} u_p + A_{pq} \frac{\partial}{\partial x} u_q = -E_{pq} u_q, \tag{44}$$

where u_p is the vector of state of n unknowns, A_{pq} is a $n \times n$ matrix with real eigenvalues and with a complete set of eigenvectors. The $n \times n$ matrix E_{pq} must be positive definite. We then rewrite system (44) in reference coordinates ξ and τ and obtain

$$\frac{\partial}{\partial t} u_q + A^*_{pq} \frac{\partial}{\partial x} u_q = -E^*_{pq} u_q \tag{45}$$

with $A^*_{pq} = \Delta t \xi_x \cdot A_{pq}$ and $E^*_{pq} = \Delta t \cdot E_{pq}$. The same steps as described in Section 2.2.1 can be applied and we finally obtain the equation system

$$(\delta_{pq}(F^1_{kl} - K^\tau_{kl}) + A^*_{pq} K^\xi_{kl} + E^*_{pq} M_{kl}) \hat{u}^i_{ql} = \delta_{pr} F^0_{km} \hat{w}^i_{rm}(t^n). \tag{46}$$

Here, δ_{pq} is the classical Kronecker symbol. The combination of the indices k, l, m for the degrees of freedom with the indices p and q for the variables can be interpreted as sub-array syntax. Using the sub-array syntax we denote the system matrix

$$Y_{pqkl} = \delta_{pq}(F^1_{kl} - K^\tau_{kl}) + A^*_{pq} K^\xi_{kl} + E^*_{pq} M_{kl} \tag{47}$$

and formally write the solution of (46) as

$$\hat{u}^i_{ql} = Y^{-1}_{pqkl} \cdot \delta_{pr} F^0_{km} \hat{w}^i_{rm}(t^n). \tag{48}$$

Eq. (46) is a local linear equation system that can be solved for each element $\mathcal{Q}_i$ independently and thus also leads to a locally implicit scheme for $u_i(\xi,\tau)$ and does not need any information from the neighboring elements.

2.2.5. General nonlinear hyperbolic systems with stiff source terms

For the construction of the space–time DG scheme for general nonlinear hyperbolic systems of conservation laws with source terms of the form (6), we also first re-write the system (6) in coordinates of the reference element as follows:

$$\frac{\partial}{\partial \tau} \mathbf{u} + \frac{\partial}{\partial \xi} \mathbf{f}^*(\mathbf{u}) = \mathbf{S}^*(\mathbf{u}) \tag{49}$$

with the modified flux and source function $\mathbf{f}^* = \mathbf{f}^*(\mathbf{u}) = \Delta t \xi_x \mathbf{f}(\mathbf{u})$ and $\mathbf{S}^* = \mathbf{S}^*(\mathbf{u}) = \Delta t \mathbf{S}(\mathbf{u})$. We then multiply with the test functions $\Phi_k(\xi,\tau)$, integrate over $\mathcal{Q}_E$ and subsequently integrate the first term containing the time derivative by parts, and introduce the corresponding time fluxes as in the linear case, in order to obtain

$$[\Phi_k, \mathbf{u}]_1 - [\Phi_k, \mathbf{w}_i]_0 - \left\langle \frac{\partial}{\partial \tau} \Phi_k, \mathbf{u} \right\rangle + \left\langle \Phi_k, \frac{\partial}{\partial \xi} \mathbf{f}^* \right\rangle = \langle \Phi_k, \mathbf{S}^* \rangle. \tag{50}$$

Plugging the ansatz for the numerical solution (22) into (50) yields the following nonlinear system of equations for the unknowns $\hat{\mathbf{u}}^i_l$:

$$[\Phi_k, \Phi_l]_1 \hat{\mathbf{u}}^i_l - [\Phi_k, \Psi_m]_0 \hat{\mathbf{w}}^i_m(t^n) - \left\langle \frac{\partial}{\partial \tau} \Phi_k, \Phi_l \right\rangle \hat{\mathbf{u}}^i_l + \left\langle \Phi_k, \frac{\partial}{\partial \xi} \mathbf{f}^*(\Phi_l \hat{\mathbf{u}}^i_l) \right\rangle - \langle \Phi_k, \mathbf{S}^*(\Phi_l \hat{\mathbf{u}}^i_l) \rangle = 0. \tag{51}$$

The necessity to solve the local nonlinear system of equations (51) adds further complications to our algorithm compared to the case of linear systems. Due to the locally implicit character of the local space–time DG scheme, the use of a Newton algorithm or other strategies for finding roots of nonlinear equation systems becomes necessary. In this paper, we apply the following strategy.

To compute the solution of (51) we first linearize the nonlinear system (49) with respect to the initial condition given by $\mathbf{w}^i(\xi,t^n)$, then we solve the resulting linear equation system (46) exactly using Gauss-Jordan elimination and obtain as result a first guess $\hat{\mathbf{u}}^{(i,1)}_l$ of the solution $\hat{\mathbf{u}}^i_l$ of (51). Linearizing about $\hat{\mathbf{u}}^{(i,1)}_l \Phi_l(\xi,1)$ and solving the resulting linear system again exactly yields the second guess values $\hat{\mathbf{u}}^{(i,2)}_l$. This procedure is usually repeated for a total number of three times. The third guess values $\hat{\mathbf{u}}^{(i,3)}_l$ are then the starting point of a standard multivariate Newton method for nonlinear systems of equations as described e.g. in chapter 9.7 of [51]. We remark that for the solution of (51) the initial guess used as input for the Newton method remains very crucial even for so-called globally convergence Newton methods as described in [51]. We note that for nonlinear systems with stiff source terms, most of the computational time of our algorithm is spent in the solution of (51). Since the authors are not experts in the field of efficiently solving nonlinear systems of equations,

there may be other, much more efficient techniques such as inexact Newton solvers to solve (51). However, the main scope of this article is not to solve (51) efficiently but to validate the general approach.

We finally would like to point out that for the special case $\mathbf{f}(\mathbf{u}) = 0$ the scheme (51) automatically reduces to a standard discontinuous Galerkin method for the nonlinear system of ordinary differential equations (ODE):

$$\frac{\partial}{\partial t}\mathbf{u} = \mathbf{S}(\mathbf{u}). \tag{52}$$

At this point, we would like to summarize again the necessary steps for our proposed explicit arbitrary high-order accurate finite volume schemes for hyperbolic systems with stiff source terms:

(I) Compute the degrees of freedom $\hat{\mathbf{w}}_l^i(t^n)$ of the weighted essentially non-oscillatory (WENO) reconstruction polynomials $\mathbf{w}_i(\xi, t^n)$ at time t^n from the given cell averages $\bar{\mathbf{u}}_i^n$ of the finite volume scheme using (14)–(18).

(II) Compute the solution $\hat{\mathbf{u}}_l^i$ of the local space–time discontinuous Galerkin method (51), where the initial condition is given by the reconstructed degrees of freedom $\mathbf{w}_l^i(\xi, t^n)$ at time t^n.

(III) Use the solution $\mathbf{u}_i(\xi, \tau) = \Phi_l(\xi, \tau)\hat{\mathbf{u}}_l^i$ to compute the arguments for the source term and the numerical flux in (10) that are needed for the explicit finite volume scheme (9). The integrals appearing in Eq. (10) are computed using classical Gaussian quadrature formulae, see e.g. [58] for details. Update the cell averages according to (9) to the new time t^{n+1} and restart with step (I).

The final scheme could also be interpreted as a method to solve the generalized Riemann problem at the cell interfaces given by the reconstruction polynomials at time t^n for the stiff balance law which follows the spirit of the original ADER schemes developed by Titarev and Toro. At the end of this section we would like to add a very important remark concerning systems of balance laws: In order to obtain a correct coupling of the flux and the source term inside the local space–time DG scheme (51) together with the finite volume discretization (9), numerical schemes of order of accuracy of at least *two* must be used, which means that the polynomial degree of the basis and test functions Φ_k must be at least *one*. This is due to the fact that the first-order version of the local space–time DG scheme, i.e. the one with polynomial degree zero for the basis and test functions Φ_k, does *not couple* source and flux in the local solution $\mathbf{u}_i(\xi, \tau)$ because the term $\langle \Phi_k, \frac{\partial}{\partial \xi}\mathbf{f}^*(\Phi_l \hat{\mathbf{u}}_l^i)\rangle$ in (51) vanishes in this case.

3. Numerical convergence studies

To assess the convergence behaviour of our method numerically, we solve the following nonlinear hyperbolic system with source terms, for which a non-trivial exact reference solution is known by construction:

$$\begin{aligned}
\frac{\partial}{\partial t}u + \frac{\partial}{\partial x}\left(\frac{1}{2}v^2\right) &= -\nu(u - u_e) + \frac{\partial}{\partial t}u_e + \frac{\partial}{\partial x}\left(\frac{1}{2}v_e^2\right),\\
\frac{\partial}{\partial t}v + \frac{\partial}{\partial x}\left(\frac{1}{2}u^2\right) &= -\nu(v - v_e) + \frac{\partial}{\partial t}v_e + \frac{\partial}{\partial x}\left(\frac{1}{2}u_e^2\right).
\end{aligned} \tag{53}$$

It is easy to see that any differentiable function pair $u_e(x,t), v_e(x,t)$ satisfies Eq. (53). For our convergence studies, we choose the following smooth reference solution:

$$u_e(x,t) = U_0 + A_u \sin(kx - \omega t), \quad v_e(x,t) = V_0 + A_v \cos(kx - \omega t). \tag{54}$$

In particular, we choose the following parameters for the reference solution used in the numerical convergence studies: $U_0 = 4$, $V_0 = 6$, $A_u = 0.1$, $A_v = 0.3$, $k = \omega = 2\pi$. Eq. (53) is solved on the computational domain $\Omega = [0;1]$ with periodic boundary conditions. The Courant number is set in the following test cases to $\mathrm{CFL} = 0.5$.

First, we assess the capability of our scheme to maintain the balance between the nonlinear advection operator on the left-hand side and the source terms on the right-hand side in the non-stiff case for $\nu = 10$. The initial conditions for u and v are in this case $u(x,0) = u_e(x,0)$ and $v(x,0) = v_e(x,0)$. We compute the problem for half a period, i.e. up to the final output time $t = 0.5$. The numerical convergence results obtained for the var-

iable v with the proposed ADER finite volume schemes from second to sixth order of accuracy in space and time are shown in Table 1, where N_G denotes the number of grid cells used to discretize the domain Ω. The errors and the associated convergence rates between two successive grid refinements are shown in L^1, L^2 and L^∞ norm. The error norms are computed numerically according to

$$\|w - v_e\|_p = \left(\int_0^1 |w(x,t) - v_e(x,t)|^p \mathrm{d}x \right)^{\frac{1}{p}}, \tag{55}$$

using Gaussian quadrature rules of appropriate order. We emphasize that the norms are computed comparing the second component of the reconstructed solution against the exact reference solution v_e. As an approximation for the infinity norm, we take the maximum of the error obtained in any of the Gaussian integration points.

The results presented in Table 1 show clearly that the method converges with the designed order of accuracy. They furthermore indicate the capability of the method to maintain a good balance between the source terms on the right-hand side of the governing equation and the nonlinear convection on the left-hand side, respectively.

Second, we assess the accuracy and the robustness of the proposed schemes in the presence of a very stiff source term. Therefore, we choose in this second test case $v = 10^8$. Since we know that the stiff relaxation source term in the governing equation (53) will cause the solution to relax to the equilibrium given by the ref-

Table 1
Numerical convergence rates for the non-stiff case ($v = 10$) obtained with ADER finite volume schemes from second to sixth order of accuracy in space and time

N_G	L^1	L^2	L^∞	$\mathcal{O}_{L^1}$	$\mathcal{O}_{L^2}$	$\mathcal{O}_{L^\infty}$
ADER-FV $\mathcal{O}2$, $(M = 1)$. $v = 10$						
8	3.1079E−02	3.3731E−02	5.3694E−02			
16	6.4558E−03	7.8656E−03	1.5286E−02	2.3	2.1	1.8
32	1.1027E−03	1.5591E−03	4.6096E−03	2.5	2.3	1.7
64	1.9859E−04	3.2959E−04	1.1626E−03	2.5	2.2	2.0
128	2.8261E−05	5.5964E−05	2.8027E−04	2.8	2.6	2.1
ADER-FV $\mathcal{O}3$, $(M = 2)$. $v = 10$						
8	4.0967E−03	5.3548E−03	1.0574E−02			
16	5.4254E−04	7.0971E−04	1.4511E−03	2.9	2.9	2.9
32	6.9171E−05	8.9516E−05	1.8292E−04	3.0	3.0	3.0
64	8.6332E−06	1.1171E−05	2.2846E−05	3.0	3.0	3.0
128	1.0816E−06	1.3965E−06	2.8546E−06	3.0	3.0	3.0
ADER-FV $\mathcal{O}4$, $(M = 3)$. $v = 10$						
4	1.5831E−02	2.0495E−02	4.1219E−02			
8	1.1568E−03	1.3030E−03	2.2840E−03	3.8	4.0	4.2
16	6.8436E−05	7.6848E−05	1.3577E−04	4.1	4.1	4.1
32	4.1739E−06	4.6990E−06	8.8561E−06	4.0	4.0	3.9
64	2.5792E−07	2.9389E−07	5.4790E−07	4.0	4.0	4.0
ADER-FV $\mathcal{O}5$, $(M = 4)$. $v = 10$						
4	1.3054E−02	1.5158E−02	2.4062E−02			
8	4.9450E−04	6.3210E−04	1.2255E−03	4.7	4.6	4.3
16	1.6178E−05	2.1234E−05	4.3206E−05	4.9	4.9	4.8
20	5.3607E−06	7.0209E−06	1.4525E−05	4.9	5.0	4.9
32	5.3921E−07	6.8677E−07	1.4518E−06	4.9	4.9	4.9
ADER-FV $\mathcal{O}6$, $(M = 5)$. $v = 10$						
4	8.3790E−03	9.9571E−03	2.2749E−02			
8	1.6979E−04	2.0617E−04	5.0498E−04	5.6	5.6	5.5
12	1.5335E−05	1.8985E−05	4.7928E−05	5.9	5.9	5.8
16	2.7810E−06	3.4639E−06	9.0072E−06	5.9	5.9	5.8
20	7.5279E−07	9.5828E−07	2.5537E−06	5.9	5.8	5.6

Table 2
Numerical convergence rates for the very stiff case ($v = 10^8$) obtained with ADER finite volume schemes from second to sixth order of accuracy in space and time

N_G	L^1	L^2	L^∞	$\mathcal{O}_{L^1}$	$\mathcal{O}_{L^2}$	$\mathcal{O}_{L^\infty}$
ADER-FV $\mathcal{O}2$, $(M = 1)$. $v = 10^8$						
8	2.9784E−02	3.0049E−02	3.4246E−02			
16	6.3522E−03	7.2830E−03	1.1337E−02	2.2	2.0	1.6
32	5.2567E−04	8.5936E−04	1.7792E−03	3.6	3.1	2.7
64	1.2096E−04	2.1170E−04	4.3802E−04	2.1	2.0	2.0
128	1.5717E−05	3.8232E−05	1.0892E−04	2.9	2.5	2.0
ADER-FV $\mathcal{O}3$, $(M = 2)$. $v = 10^8$						
8	3.5814E−03	5.0870E−03	9.2163E−03			
16	4.5652E−04	6.7004E−04	1.2552E−03	3.0	2.9	2.9
32	5.7309E−05	8.4607E−05	1.6027E−04	3.0	3.0	3.0
64	7.1382E−06	1.0613E−05	2.0140E−05	3.0	3.0	3.0
128	8.9658E−07	1.3275E−06	2.5379E−06	3.0	3.0	3.0
ADER-FV $\mathcal{O}4$, $(M = 3)$. $v = 10^8$						
4	1.4142E−02	1.9636E−02	3.8569E−02			
8	1.0485E−03	1.2385E−03	2.3951E−03	3.8	4.0	4.0
16	6.4253E−05	7.5030E−05	1.4553E−04	4.0	4.0	4.0
32	3.9752E−06	4.6373E−06	9.0331E−06	4.0	4.0	4.0
64	2.4920E−07	2.8917E−07	5.5709E−07	4.0	4.0	4.0
ADER-FV $\mathcal{O}5$, $(M = 4)$. $v = 10^8$						
4	1.3054E−02	1.5158E−02	2.4062E−02			
8	4.9450E−04	6.3210E−04	1.2255E−03	4.7	4.6	4.3
16	1.6179E−05	2.1235E−05	4.3216E−05	4.9	4.9	4.8
32	5.3935E−07	6.8713E−07	1.4690E−06	4.9	4.9	4.9
64	2.0147E−08	2.5747E−08	6.4216E−08	4.7	4.7	4.5
ADER-FV $\mathcal{O}6$, $(M = 5)$. $v = 10^8$						
4	8.3790E−03	9.9571E−03	2.2749E−02			
8	1.6980E−04	2.0617E−04	5.0498E−04	5.6	5.6	5.5
12	1.5336E−05	1.8986E−05	4.7918E−05	5.9	5.9	5.8
16	2.7812E−06	3.4641E−06	8.9977E−06	5.9	5.9	5.8
20	7.5301E−07	9.5840E−07	2.5566E−06	5.9	5.8	5.6

erence solution u_e, v_e from any initial condition, we choose a constant initial condition $u(x,0) = 10$, $v(x,0) = 2$, which is far from the equilibrium u_e, v_e and as a consequence in the first time steps the source is very stiff. Once the equilibrium $u = u_e, v = v_e$ has been reached, the scheme must be able to maintain it. The numerical convergence rates obtained for variable v with ADER finite volume schemes from second to sixth order for this very stiff case ($v = 10^8$) are shown in Table 2. From the results we can clearly conclude that the method is at the same time able to treat stiff source terms robustly and maintains an excellent balance between flux divergence and source term at the designed order of accuracy in space and time. To our knowledge, this is the first finite volume scheme ever presented in the research literature on stiff source terms that achieves arbitrary high order of accuracy in space and time. This is, of course, only valid for sufficiently smooth solutions.

4. Applications

4.1. Model system with linear flux and nonlinear source term

We consider the following class of linear advection systems with nonlinear relaxation:

$$\begin{cases} \frac{\partial}{\partial t} u + \frac{\partial}{\partial x} v = 0, \\ \frac{\partial}{\partial t} v + \frac{\partial}{\partial x} u = -\frac{1}{\epsilon} \frac{v}{\alpha(u)}, \end{cases} \tag{56}$$

where ϵ is a positive parameter and $\alpha(u)$ is any given function which satisfies $\alpha(u) > 0\ \forall u$ in the domain of interest and does not depend on ϵ. System (56) can be seen as a dimensionless system where ϵ is the ratio between the characteristic time of the relaxation process over the characteristic time of the pure advection process. If the relaxation process is much faster than the advection process, namely if $\epsilon \ll 1$ which corresponds to the stiff case, it is possible to obtain the asymptotic limit of the system. An asymptotic expansion of the relaxating variable formally reads as

$$v = v_0 + \epsilon v_1 + \mathcal{O}(\epsilon^2), \tag{57}$$

where v_0 and v_1 are unknown functions of x and t. Here we recall that expansion (57) should not be interpreted as a convergent mathematical series, but as a truncated formal expansion. Injecting (57) into system (56), we find iteratively that $v_0 = 0$ and $v_1 = -\alpha(u)\frac{\partial}{\partial x}u$ for an arbitrary small value of ϵ. Thus, as $\epsilon \to 0$, variable v is given by the following equation:

$$v = -\epsilon\alpha(u)\frac{\partial}{\partial x}u + \mathcal{O}(\epsilon^2) \tag{58}$$

and the asymptotic limit of system (56) reads as

$$\frac{\partial}{\partial t}u = \epsilon\frac{\partial}{\partial x}\left[\alpha(u)\frac{\partial}{\partial x}u\right] + \mathcal{O}(\epsilon^2), \tag{59}$$

which is a nonlinear diffusion equation.

Example 1 ($\alpha(u) = 1$). We consider first the linear case $\alpha(u) = 1$. According to (59), as $\epsilon \to 0$, system (56) reduces to the well-known heat equation:

$$\frac{\partial}{\partial t}u = \epsilon\frac{\partial^2}{\partial x^2}u, \tag{60}$$

where ϵ plays the role of a (small) diffusion coefficient. Suppose that the domain of interest is $x \in \mathbb{R}$ and that an initial condition $u(x,0) = u_0(x)$ is given. Then an analytical solution of Eq. (60) is known, namely the following Green function:

$$u(x,t) = \frac{1}{\sqrt{4\pi\epsilon t}}\int_{-\infty}^{+\infty} u_0(\xi)\mathrm{e}^{-\frac{(x-\xi)^2}{4\epsilon t}}\mathrm{d}\xi. \tag{61}$$

We now solve the system (56) up to the final output time $t = 50$ in the computational domain $\Omega = \left[-\frac{1}{2};\frac{1}{2}\right]$ with $\alpha(u) = 1$ using ADER-FV schemes from second to fifth order of accuracy on 100 cells. The local space–time DG scheme for linear systems can be directly applied according to (46). We take a stiffness parameter of $\epsilon = 10^{-4}$ and as initial condition we choose

$$u_0(x) = \begin{cases} 1000 & \text{if } x \leqslant 0, \\ 1 & \text{if } x > 0. \end{cases} \tag{62}$$

The boundary conditions are chosen to be transmissive. The analytical solution of the heat equation (60) with the initial condition (62) is given in terms of the error function $\mathrm{erf}(x)$ at $t = 50$ with $\epsilon = 10^{-4}$ as

$$u(x,50) = \frac{1001}{2} - \frac{999}{2}\cdot\mathrm{erf}(5\sqrt{2}x), \tag{63}$$

against which the numerical solutions will be compared. The Courant number is set in all computations to $\mathrm{CFL} = \Delta t/\Delta x = 0.9$. The final output time $t = 50$ is quite large and is reached with the chosen combination of mesh and Courant number after 5556 iterations. Hence, we expect that the low-order schemes will add more spurious numerical diffusion in this test case compared to the high-order schemes since we compute a large number of time steps. This conjecture is indeed confirmed by our numerical results that are depicted in Fig. 2. We can see that generally all the schemes capture the exact reference solution (63) quite well. However, the higher-order schemes produce better results than the lower-order methods. This means that even in the diffusion limit of the stiff system (56) higher-order schemes may produce better results than lower-order meth-

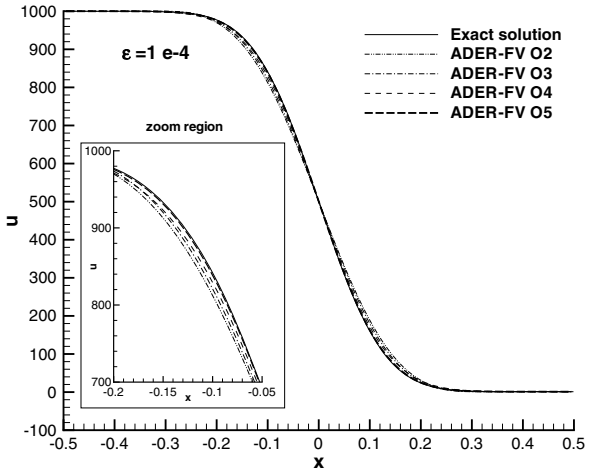

Fig. 2. Exact and numerical solutions obtained on 100 cells using ADER-FV schemes of second to fifth order of accuracy in space and time for the model system with linear flux and stiff linear source ($\epsilon = 10^{-4}$) at time $t = 50$.

ods. We finally would like to emphasize that our numerical results have been obtained using a standard *explicit* one-step high-order finite volume scheme, where we only use a particular procedure in order to predict the local time-evolution of the reconstructed polynomials. This is achieved via our new local space–time discontinuous Galerkin scheme proposed in this article. The rest of the finite volume scheme is standard.

Example 2 ($\alpha(u) = u(1-u)$). We now consider a special nonlinear case, namely $\alpha(u) = u(1-u)$. Hypothesis $\alpha(u) > 0$ is valid if and only if $u \in]0;1[$. In this region, according to (59), as $\epsilon \to 0$, system (56) reduces to the following nonlinear diffusion equation:

$$\frac{\partial}{\partial t}u = \epsilon \frac{\partial}{\partial x}\left[u(1-u)\frac{\partial}{\partial x}u\right]. \tag{64}$$

Suppose that the domain of interest is $\Omega = [-0.5; 0.5]$ for a given $L > 0$, and that Neumann boundary conditions $\left(\frac{\partial}{\partial x}u\right)(-0.5,t) = \left(\frac{\partial}{\partial x}u\right)(0.5,t) = 0$ are imposed $\forall t > 0$. Then, for the initial condition we use

$$u(x,0) = \begin{cases} 1^{-}\text{if } x \leqslant 0, & \text{where } 1^{-} = \lim\limits_{\delta\to 0} 1-\delta, \\ 0^{+}\text{if } x > 0, & \text{where } 0^{+} = \lim\limits_{\delta\to 0} \delta, \end{cases} \tag{65}$$

where for small $\delta > 0$, an analytical solution of Eq. (64) is known, namely

$$u(x,t) = \min\left(1, \max\left(0, \frac{1}{2}\left(1 - \frac{x}{\sqrt{\epsilon t}}\right)\right)\right). \tag{66}$$

We solve this test problem for $\delta = 10^{-6}$ with ADER-FV schemes of second, third and fifth order of accuracy using 100 cells in the computational domain Ω up to time $t = 10$ with $\epsilon = 10^{-3}$ and a Courant number of CFL = 0.25. The numerical results and the exact reference solution for the stiff limit are depicted in Fig. 3. We note that all methods agree very well with the reference solution and that even in this case, with discontinuities in the first derivative of the solution, we can clearly see an improvement with increasing order of accuracy.

4.2. Model system with nonlinear flux and linear source term

We now consider the following class of nonlinear advection systems with linear relaxation:

$$\begin{cases} \frac{\partial}{\partial t}u + \frac{\partial}{\partial x}v = 0, \\ \frac{\partial}{\partial t}v + \frac{\partial}{\partial x}f(u) = -\frac{1}{\epsilon}v, \end{cases} \tag{67}$$

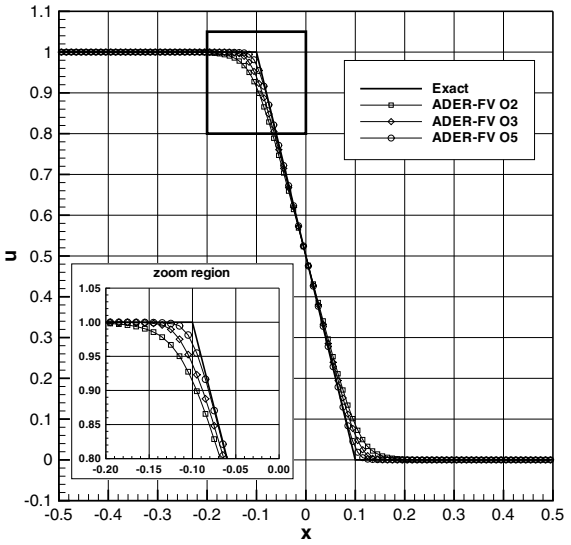

Fig. 3. Exact and numerical solutions obtained on 100 cells using ADER-FV schemes of second, third and fifth order of accuracy in space and time for the model system with linear flux and stiff nonlinear source ($\epsilon = 10^{-3}$) at time $t = 10$.

where ϵ is a positive parameter and $f(u)$ is any given function which satisfies $f'(u) \geqslant 0\ \forall u$ in the domain of interest and does not depend on ϵ. Injecting asymptotic expansion (57) into system (67), we find iteratively that $v_0 = 0$ and $v_1 = -f'(u)\frac{\partial}{\partial x}u$ for an arbitrary small value of ϵ. Thus, as $\epsilon \to 0$, variable v is given by the following equation:

$$v = -\epsilon f'(u)\frac{\partial}{\partial x}u + \mathcal{O}(\epsilon^2) \tag{68}$$

and the asymptotic limit of system (67) reads as

$$\frac{\partial}{\partial t}u = \epsilon\frac{\partial}{\partial x}\left[f'(u)\frac{\partial}{\partial x}u\right] + \mathcal{O}(\epsilon^2), \tag{69}$$

which is a nonlinear diffusion equation. Note that in the previous section, we had $\alpha(u) > 0$, while here we have $f'(u) \geqslant 0$.

Example 3. $f'(u) = u(1-u)$. We consider the special nonlinear case $f'(u) = u(1-u)$, which leads to $f(u) = \frac{1}{2}u^2 - \frac{1}{3}u^3$. The hypothesis $f'(u) > 0$ is verified if and only if $u \in [0;1]$. In this region, according to (69), as $\epsilon \to 0$, system (67) reduces to the nonlinear diffusion Eq. (64). Suppose that the domain of interest is $x \in [-0.5; 0.5]$ for a given $L > 0$, and that Neumann boundary conditions $\left(\frac{\partial}{\partial x}u\right)(-0.5, t) = \left(\frac{\partial}{\partial x}u\right)(0.5, t) = 0$ are imposed $\forall t > 0$. Then, an analytical solution of Eq. (64) is (66), which is compatible with the initial condition:

$$u(x,0) = \begin{cases} 1^- & \text{if } x \leqslant 0, \quad \text{where } 1^- = \lim\limits_{\delta\to 0} 1-\delta, \\ 0^+ & \text{if } x > 0, \quad \text{where } 0^+ = \lim\limits_{\delta\to 0}\delta. \end{cases} \tag{70}$$

We solve this test problem for $\delta = 10^{-4}$ with ADER-FV schemes of second, third and fifth order of accuracy using 100 cells in the computational domain Ω up to time $t = 10$ with $\epsilon = 10^{-3}$ and a Courant number of CFL = 0.25. The numerical results and the exact reference solution for the stiff limit are depicted in Fig. 4. As in the previous test problem, all methods agree again very well with the reference solution and an improvement with increasing order of accuracy is also visible.

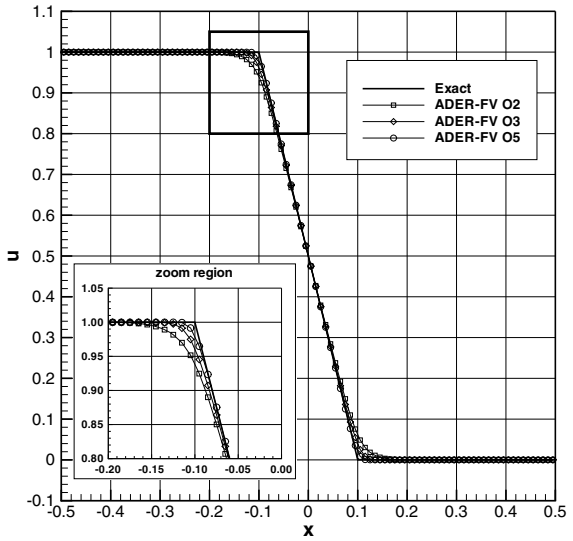

Fig. 4. Exact and numerical solutions obtained on 100 cells using ADER-FV schemes of second, third and fifth order of accuracy in space and time for the model system with nonlinear flux and stiff linear source ($\epsilon = 10^{-3}$) at time $t = 10$.

4.3. Euler equations with stiff friction

In this section, we apply our method to the Euler equations of compressible gas dynamics with stiff friction. The full Euler system with friction reads as (6) with the vector of conservative variables $\mathbf{u}$, the flux $\mathbf{f}(\mathbf{u})$ and the (stiff) source term $\mathbf{S}(\mathbf{u})$ as

$$\mathbf{u} = \begin{pmatrix} \rho \\ \rho u \\ \rho E \end{pmatrix}, \quad \mathbf{f}(\mathbf{u}) = \begin{pmatrix} \rho u \\ \rho u^2 + p \\ u(\rho E + p) \end{pmatrix}, \quad \mathbf{S}(\mathbf{u}) = -v \begin{pmatrix} 0 \\ \rho u \\ \rho u^2 \end{pmatrix}. \tag{71}$$

The system still needs to be closed by an equation of state (EOS) of the form $p = p(\mathbf{u})$. For the following numerical calculations we consider a computational domain $\Omega = [0; 1]$ with the Dirichlet boundary conditions $\mathbf{u}(0, t) = \mathbf{u}(0, 0)$ and $\mathbf{u}(1, t) = \mathbf{u}(1, 0)$ and the initial condition

$$\mathbf{u}(x, 0) = \begin{cases} (1.65, 0, 5.039849068) & \text{if } x \leqslant 0.25, \\ (0.01, 0, 0.003962233) & \text{if } x > 0.25. \end{cases} \tag{72}$$

For the stiffness parameter v we take

$$v(x, t) = \begin{cases} 0 & \text{if } x \leqslant 0.25, \\ 1500 & \text{if } x > 0.25, \end{cases} \tag{73}$$

which means that we solve the Euler equations *without* any friction in the left quarter of Ω ($x \in [0; 0.25]$) and with *stiff* friction in the region $x \in [0.25; 1]$. This setup corresponds to an interface of an inviscid compressible gas with a porous medium into which the gas may penetrate. For all the following computations we set the Courant number to CFL = 0.9.

4.3.1. Isentropic Euler system with stiff friction

Under the assumption that the flow is completely isentropic, we can write the equation of state as

$$p(\mathbf{u}) = k\rho^{\gamma}. \tag{74}$$

In this case, the pressure does not depend on the total energy ρE and thus the energy equation in (6) and (71) can be omitted. We set $k = 1$ and $\gamma = 1.4$. We solve (6) with (71) and the EOS (74) up to $t = 2.0$ using 100 cells and ADER-FV schemes from second to fourth order of accuracy. The reference solution is computed with a

second-order ADER-FV scheme on 10,000 cells. The results are depicted in Fig. 5(a). We clearly see that on a fixed grid the diffusion limit of the Euler equations is captured better by the higher-order schemes. Although the results of the second-order method are still of acceptable accuracy, we nevertheless observe that the second-order method adds too much numerical diffusion. A very similar test case has previously been proposed by Bouchut et al. [6]. Unfortunately they did not specify all parameters of their test problem. Especially, the initial and boundary conditions were not given, so it was not possible to compute exactly the same test case. However, the results are qualitatively similar compared to ours.

4.3.2. Full Euler system with stiff friction

Using the ideal gas law, the equation of state reads as

$$p(\mathbf{u}) = (\gamma - 1)\left(\rho E - \frac{1}{2}\rho u^2\right), \tag{75}$$

where $\gamma = 1.4$. In this case, we must consider the full Euler system including the energy equation. In the initial condition (72) the total energy ρE is chosen such that the pressure according to (75) is equal to the pressure obtained in the isentropic case from Eq. (74). We therefore expect the results to be very similar to the previous ones. Hence, we solve (6) with (71) and the EOS (75) up to $t = 2.0$ using the initial condition (72). The computational domain is discretized with 100 cells using ADER-FV schemes from second to fourth order of accuracy. The reference solution is computed again with a second-order ADER-FV scheme on 10,000 cells. The results are depicted in Fig. 5(b). Similar to the isentropic case, we observe that also the diffusion limit of the full Euler equations is captured better by the higher-order schemes.

We finally would like to remark that even some first-order numerical methods designed for stiff systems of balance laws may encounter problems with this test case for the full Euler equations since they may produce negative values for the total energy ρE.

4.4. The relaxation system of Jin and Xin

The relaxation system of Jin and Xin [37] reads as follows:

$$\begin{cases} \frac{\partial}{\partial t}\mathbf{u} + \frac{\partial}{\partial x}\mathbf{v} = 0, \\ \frac{\partial}{\partial t}\mathbf{v} + A\frac{\partial}{\partial x}\mathbf{u} = -\frac{1}{\epsilon}(\mathbf{v} - \mathbf{f}(\mathbf{u})), \end{cases} \tag{76}$$

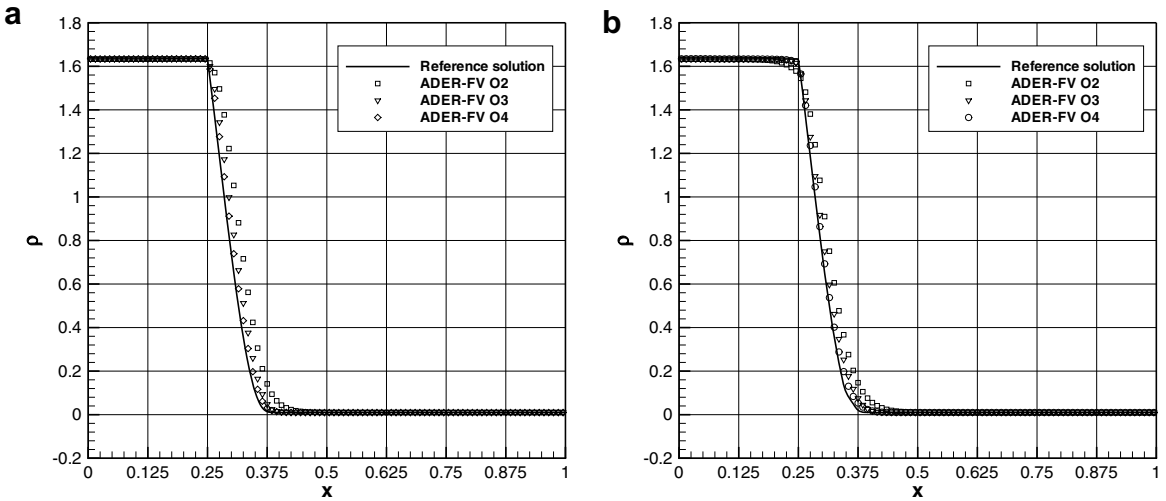

Fig. 5. Reference solution and numerical solutions at time $t = 2$ obtained on 100 cells using ADER-FV schemes of second, third and fourth order of accuracy in space and time for the Euler system with stiff friction. (a) Isentropic Euler system (left) and (b) full Euler system with ideal gas EOS (right).

where $\mathbf{f}(\mathbf{u})$ is a given function, ϵ is a positive arbitrarily small parameter and A is a constant matrix. The advection part of this system is linear, while the relaxation part is not linear in general, due to the presence of $\mathbf{f}(\mathbf{u})$. It is easy to check that the asymptotic limit of system (76) is

$$\frac{\partial}{\partial t}\mathbf{u} + \frac{\partial}{\partial x}\mathbf{f}(\mathbf{u}) = \epsilon \frac{\partial}{\partial x}\left[(A - J^2(\mathbf{u}))\frac{\partial}{\partial x}\mathbf{u}\right], \tag{77}$$

where $J = \frac{\partial \mathbf{f}}{\partial \mathbf{u}}$. System (77) is a hyperbolic system of conservation laws with nonlinear diffusion if and only if

$$A \geqslant J^2(\mathbf{u}) \quad \forall \mathbf{u}. \tag{78}$$

We now apply our proposed ADER finite volume schemes for hyperbolic systems with stiff source terms to the relaxation system of Jin and Xin with the following definitions of the vector $\mathbf{u}$ and the flux function $\mathbf{f}(\mathbf{u})$ appearing in the source term:

$$\mathbf{u} = (\rho, \rho u, \rho E), \quad \mathbf{f}(\mathbf{u}) = (\rho u, \rho u^2 + p, u(\rho E + p)) \tag{79}$$

with the equation of state that closes the system

$$p = (\gamma - 1)\left(\rho E - \frac{1}{2}\rho u^2\right). \tag{80}$$

With this choice Eq. (76) converges to the compressible Euler equations in the stiff limit. The stiffness parameter $v = 1/\epsilon$ is set in all the following test cases to $v = 10^{12}$, which leads to a very stiff source term. The matrix A is chosen to be the simple diagonal matrix $A = \mathrm{diag}(a_m, a_m, a_m)$, which is kept constant in space and time.

4.4.1. Shock tube problems

We consider initial value problems for (76) where the initial condition for $\mathbf{u}$ has the form

$$\mathbf{u}(x,0) = \begin{cases} (\rho_L, (\rho u)_L, (\rho E)_L) & \text{if } x \leqslant x_c, \\ (\rho_R, (\rho u)_R, (\rho E)_R) & \text{if } x > x_c. \end{cases} \tag{81}$$

The initial condition for $\mathbf{v}$ is simply $\mathbf{v}(x,0) = 0$ and we use Dirichlet boundary conditions that are consistent with the initial condition. For the Euler equations of compressible gas dynamics the exact solution of those Riemann problems can be computed analytically and will serve in the following for validation of our numerical method when applied to the relaxation system of Jin and Xin. We compute the solution of the initial value problem (76) and (81) using second- to fourth-order ADER-FV schemes for six different cases of shock tube problems. All initial conditions as well as the final output times t_{end} and the initial position of the discontinuity x_c are listed in Table 3. The values a_m defining the matrix A are given for each test case in Table 4. For all computations we use a constant Courant number of CFL = 0.75. The exact solution and the numerical solutions obtained by our proposed method are shown for all six shock tube problems in Figs. 6–8, where also the number of mesh cells is indicated. For most of the test cases we note an excellent agreement with the exact solution and most of the numerical solutions are monotone, thanks to the nonlinear WENO reconstruction procedure. We note that the reconstruction is done in the characteristic variables of the compressible Euler equations and *not* in the characteristic variables of the advection operator of the relaxation system of Jin and Xin. This is necessary to suppress unphysical oscillations. Using this particular characteristic reconstruction, small spurious oscillations are only visible for shock tube problems number two and four. We note that

Table 3
Initial states left and right, simulation end times and initial position x_c of the discontinuity for the 1D shock tube problems computed with the relaxation system of Jin and Xin

Case	ρ_L	u_L	p_L	ρ_R	u_R	p_R	t_{end}	x_c
1	1.0	0.75	1.0	0.125	0.0	0.1	0.20	0.5
2	1.0	−2.0	0.4	1.0	2.0	0.4	0.15	0.5
3	0.445	0.698	3.528	0.5	0.0	0.571	0.14	0.5
4	5.99924	19.5975	460.895	5.99242	−6.19633	46.0950	0.035	0.4
5	1.0	0.0	1000	1.0	0.0	0.01	0.012	0.5
6	1.0	−19.59745	1000	1.0	−19.59745	0.01	0.012	0.8

Table 4
Entries a_m of the diagonal matrix A for the 1D shock tube problems

Case	1	2	3	4	5	6
a_m	7	12	12	900	1500	9000

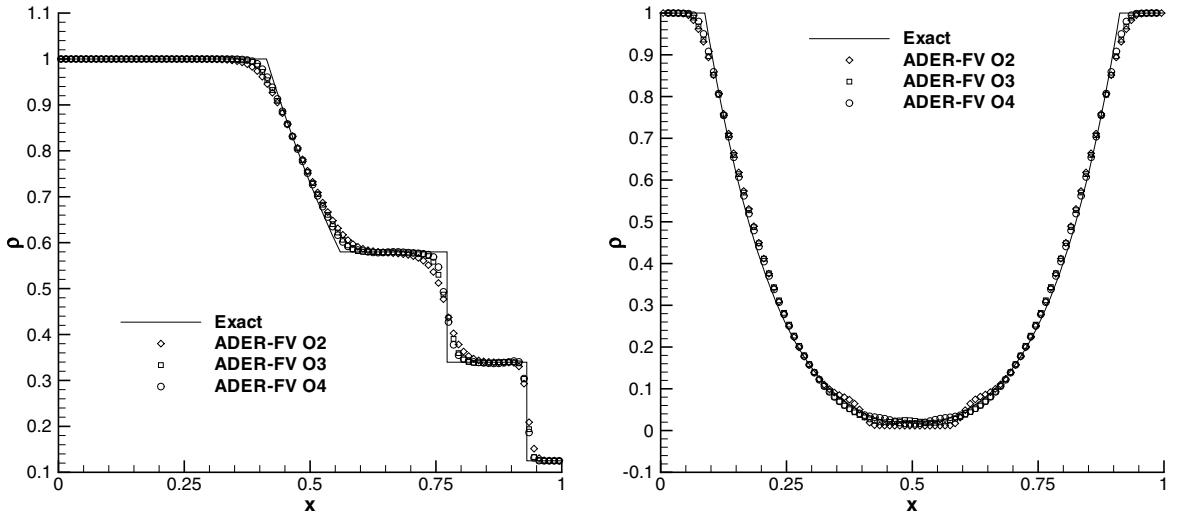

Fig. 6. Exact and numerical solutions for shock tube problems number one (left) and two (right), obtained with the relaxation system of Jin and Xin on 100 cells.

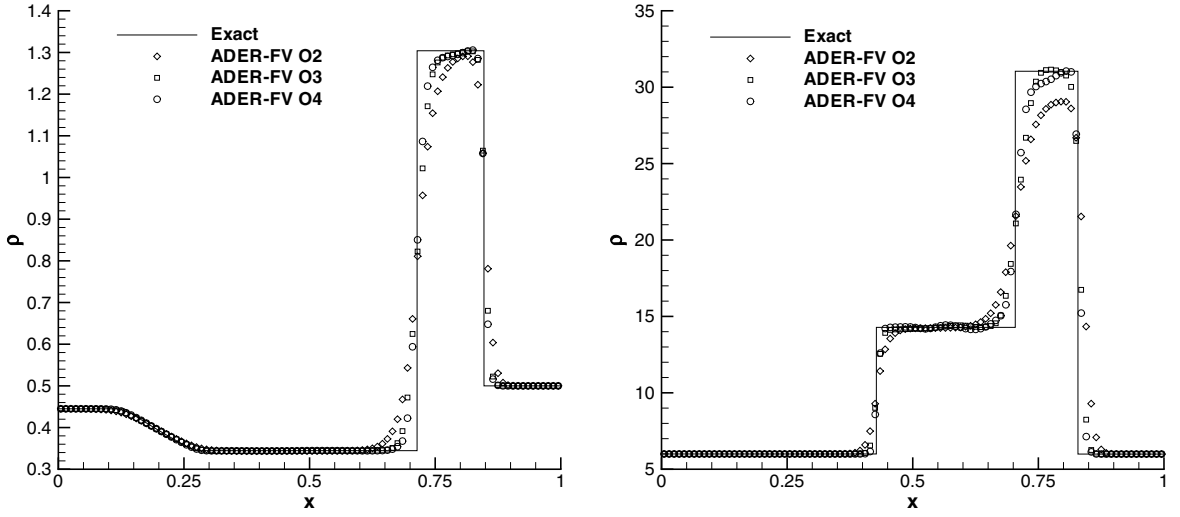

Fig. 7. Exact and numerical solutions for shock tube problems number three (left) and four (right), obtained with the relaxation system of Jin and Xin on 100 cells.

these test cases can be even difficult to compute with standard high-order finite volume schemes for the compressible Euler equations. Much more numerical difficulties arise in the relaxation system of Jin and Xin due to the very stiff source term. However, the numerical results confirm that our method produces essentially non-oscillatory results, maintains high accuracy even for hyperbolic systems with stiff source terms and has the correct behaviour in the stiff limit.

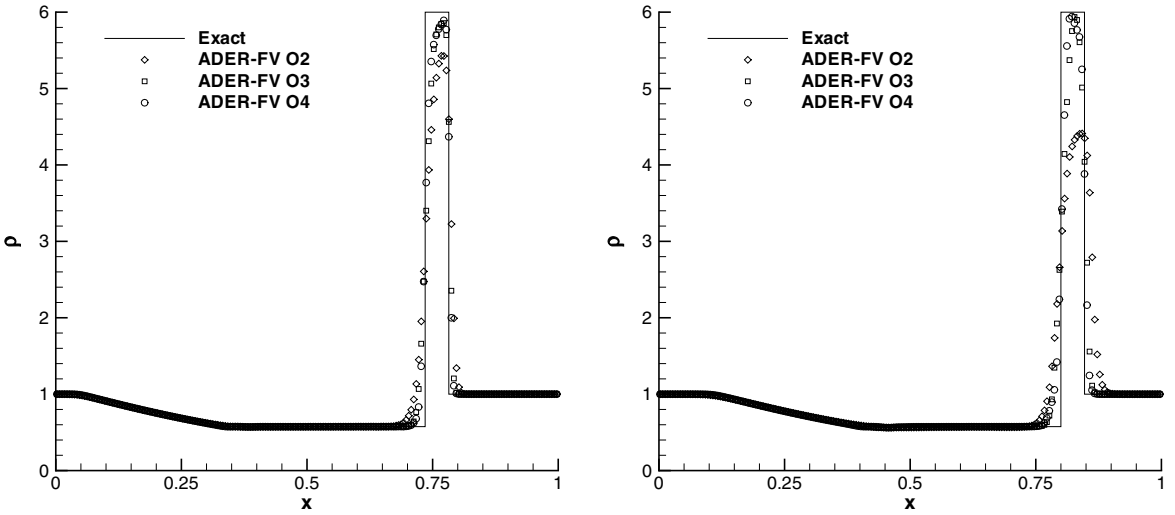

Fig. 8. Exact and numerical solutions for shock tube problems number five (left) and six (right), obtained with the relaxation system of Jin and Xin on 200 cells.

4.4.2. Shock–density interaction

We now consider a test problem proposed originally by Shu and Osher [56] for the compressible Euler equations in the more general framework of the stiff relaxation system of Jin and Xin (76) in order to show the advantages of high-order methods. We emphasize that for this test case we solve the stiff relaxation system of Jin and Xin (76) and *not* the classical Euler equations of compressible gas dynamics. The computational domain is $\Omega = [-5; 5]$ and the initial condition for $\mathbf{u}$ is given by

$$(\rho, u, p)(x, 0) = \begin{cases} (3.8571, 2.6294, 10.333) & \text{if } x < -4, \\ (1 + 0.2\sin(5x), 0, 1) & \text{if } x \geqslant -4. \end{cases} \tag{82}$$

Dirichlet boundaries consistent with the initial condition are imposed. Furthermore we set $\mathbf{v}(x, 0) = 0$. This leads to a shock wave with Mach number $M = 3$ running into the sinusoidal density fluctuation. The interaction

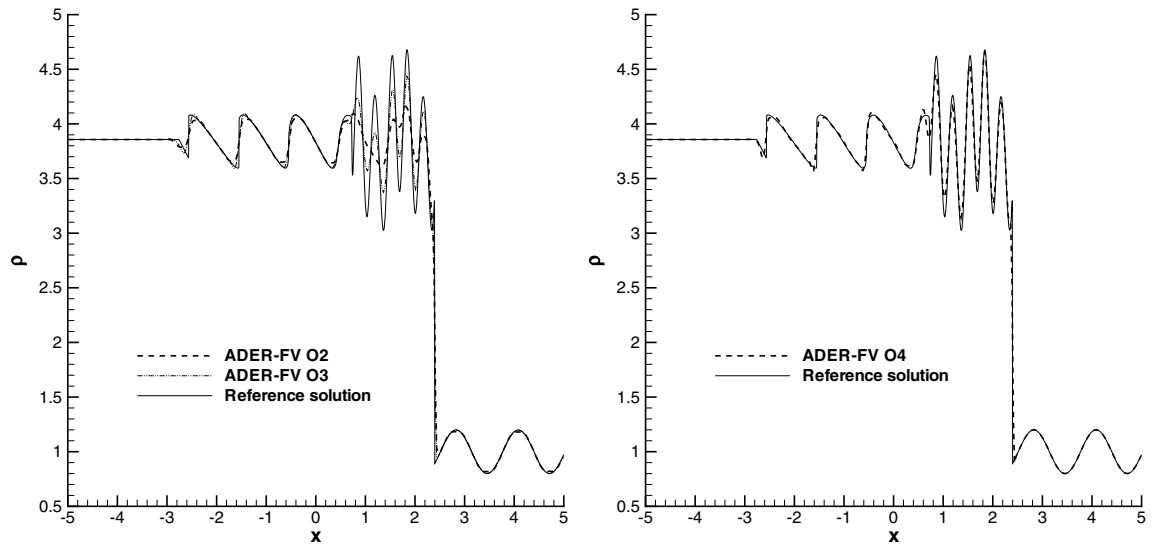

Fig. 9. Reference solution and numerical solutions at $t = 1.8$ for the shock–density interaction test case obtained with the relaxation system of Jin and Xin on 400 cells using ADER-FV schemes of second, third and fourth order of accuracy.

of the shock with the density fluctuation generates sound waves and high-frequency entropy fluctuations that are very difficult to capture with low-order schemes on coarse meshes. In Fig. 9, we show the numerical results obtained with ADER-FV schemes from second to fourth order of accuracy on 400 cells at the final output time $t = 1.8$. We choose $a_m = 25$ and a Courant number of CFL $= 0.75$.

One can clearly see that the second-order method is not at all able to resolve the high frequency entropy waves. The third-order scheme already resolves the whole frequency content but is still too dissipative since the amplitudes of the entropy waves are not yet captured, see Fig. 9 on the left. Only the fourth-order scheme is able to resolve the whole solution quite well on this relatively coarse mesh, see Fig. 9 on the right. The reference solution was computed using a second-order TVD finite volume scheme for the compressible Euler equations on 10,000 cells.

4.5. The scalar model problem of LeVeque and Yee

The model problem proposed by LeVeque and Yee [41] is a scalar linear advection problem with a nonlinear reaction source term, which can be stiff. The governing PDE reads as

$$\frac{\partial}{\partial t}u + \frac{\partial}{\partial x}u = -\nu u(u-1)\left(u - \frac{1}{2}\right), \tag{83}$$

where ν is a given positive coefficient. The computational domain is $\Omega = [0;1]$ with transmissive boundary conditions. The following initial condition is considered:

$$u(x,0) = \begin{cases} 1 & \text{if } x \leqslant 0.3, \\ 0 & \text{if } x > 0.3. \end{cases} \tag{84}$$

With this particular initial condition, the source term is zero. Thus, an analytical solution of problem (83) and (84) is known, namely: $u(x,t) = u(x-t,0)$, which means that the initial profile of u is advected with constant speed 1. LeVeque and Yee have pointed out that neither a Mac Cormack predictor–corrector method, nor a Strang splitting method give the physically correct advection speed in the stiff case. We further note that also standard ADER finite volume schemes [65,60] using the usual Cauchy–Kovalewski procedure instead of the proposed local space–time discontinuous Galerkin scheme to compute $u_i(\xi,\tau)$ from the reconstructed polynomials $w_i(\xi,t^n)$ are not able to solve this problem since they cannot handle stiff source terms. Following LeVeque and Yee we now solve the above mentioned test problem up to $t = 0.3$ using 100 cells and a Courant number of CFL $= 0.75$, taking the following values for the stiffness parameter: $\nu = 1$, $\nu = 10$, $\nu = 100$, $\nu = 1000$. The numerical results obtained with our new ADER-FV schemes from second to sixth order of accuracy are depicted in Fig. 10 for the non-stiff as well as for the stiff cases. We note an excellent agreement with the exact solution in all cases. In particular, the advection speed of $a = 1$ seems to be captured correctly. Furthermore, we can clearly see that our numerical solution is essentially non-oscillatory and that the resolution of the discontinuity is improved in the non-stiff case when using higher-order schemes. For the stiff case, we observe less numerical diffusion than in the non-stiff case. This is due to the reaction source term, which has two stable equilibrium solutions at $u = 0$ and at $u = 1$. Any numerical dissipation generated by the numerical scheme will lead to a smearing of the discontinuity and will subsequently lead to intermediate values of u that do not correspond to either of the stable equilibria. The stiff reaction source term will immediately try to push the solution back towards the closest equilibrium, which in the end leads to a generally sharper profile for the stiff case compared to the non-stiff case. The fact that we obtain the correct propagation speed can be probably explained by the following reasoning: It has been reported in the literature that numerical problems induced by stiff reaction source terms can be cured using high resolution methods together with either locally refined meshes via an AMR technique or front tracking approaches, see e.g. [29,40,7]. Instead of these techniques we are using for this test case throughout very high-order accurate numerical methods that exhibit generally only few numerical diffusion. Furthermore, the proposed one-step time discretization allows us to use the nonlinear WENO reconstruction operator, which induces a certain amount of extra numerical diffusion compared to a non-monotone reconstruction, only once per time-step. According to previous publications on ADER and Lax–Wendroff type one-step time discretizations for WENO and DG schemes this results in less numerical

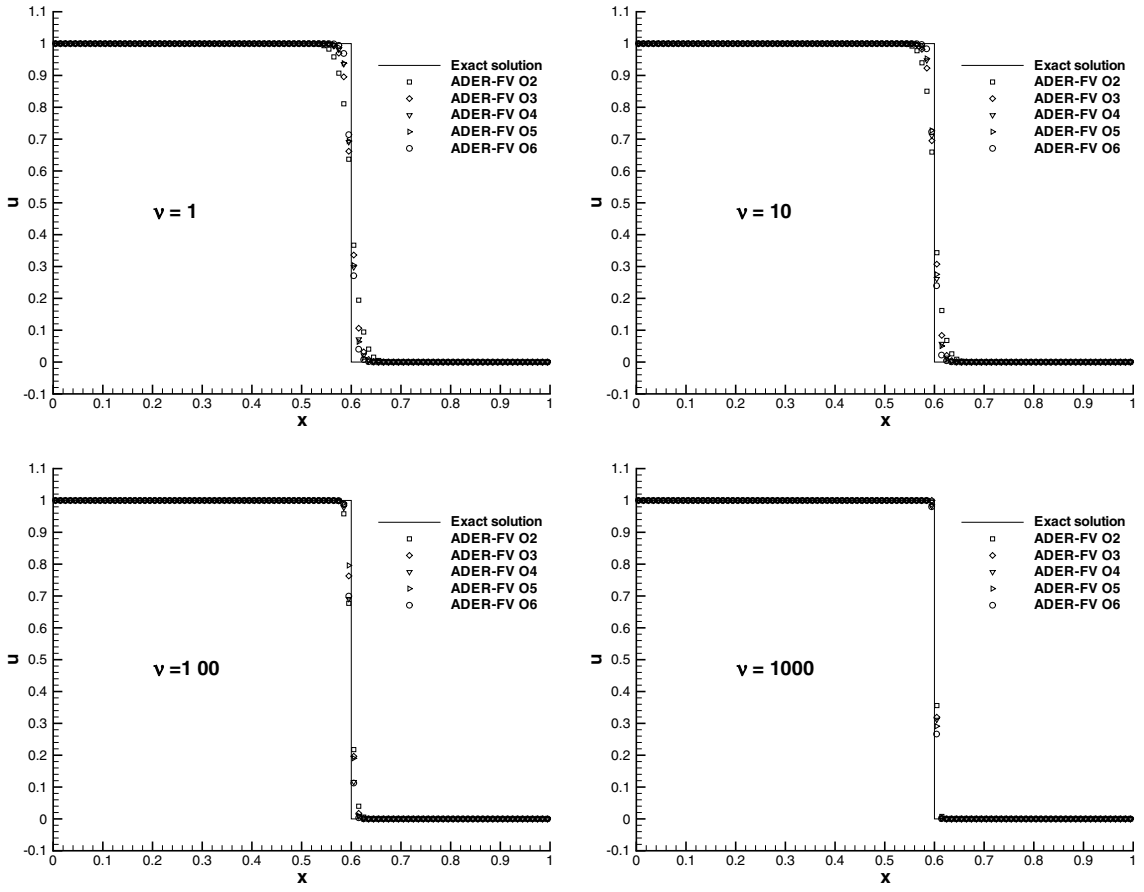

Fig. 10. Exact solution and numerical solutions for the model problem of LeVeque and Yee at $t = 0.3$ using 100 cells for the non-stiff case (top row) and the stiff case (bottom row). $v = 1$ (top left), $v = 10$ (top right), $v = 100$ (bottom left), $v = 1000$ (bottom right).

diffusion compared to classical TVD Runge–Kutta type time discretizations for WENO and DG schemes [15,53,52,60,59]. Another feature of our particular time discretization is the fact that the flux and the source term are intrinsically coupled within the local space–time DG scheme. Via this approach, the influence of the source term is present in the numerical flux function as well as the influence of the convection is present in the numerical source term.

5. Summary and conclusions

In this article, we have developed a new explicit unsplit essentially non-oscillatory one-step finite volume scheme of arbitrary high order of accuracy in space and time for nonlinear hyperbolic systems with stiff source terms. In continuity with previous work of the authors on schemes of arbitrary high order of accuracy in space and time, we call our new method also ADER (**a**rbitrary high-order **der**ivatives) finite volume scheme. The spatial reconstruction polynomials obtained from the particular WENO reconstruction operator are used as initial conditions for the proposed local space–time discontinuous Galerkin scheme which solves an initial value problem for the governing PDE *locally* inside each element without considering the neighboring elements. The local space–time DG scheme leads in general to a *local* system of nonlinear equations that has to be solved individually for each element. In this article, we use a standard globally convergent Newton algorithm [51] to solve the problem in the nonlinear case. As initial guess we solve an associated linear problem after linearization of the governing PDE. We emphasize that the local space–time DG scheme is the only locally implicit part appearing in the proposed ADER-FV schemes. The resulting ADER finite volume scheme, built upon the solution of the local space–time DG scheme, is then completely explicit. Compared

to previous ADER-FV schemes for hyperbolic systems with non-stiff source terms, the new local space–time DG scheme has replaced the usual Cauchy–Kovalewski procedure, which is not able to treat stiff problems. The rest of the scheme remains the same.

We have shown via formal asymptotic expansions that the new local space–time DG scheme is able to capture correctly the stiff limit in the case of a linear scalar PDE with stiff source term and that it is also asymptotic preserving (AP) for the case of a stiff linear two-equation model system.

Numerical convergence studies for our proposed method have been carried out up to sixth order of accuracy in space and time for a nonlinear hyperbolic system with source terms. A non-stiff case and also a very stiff case have been considered. The ADER-FV schemes then have been applied to several stiff linear and nonlinear model systems. In all the cases our schemes were able to capture very well the stiff limit of these equations and to maintain also the monotonicity of the solution, even using schemes of very high order of accuracy. Usually, the results obtained with the higher-order schemes were better than the results obtained with the lower-order methods, even for test problems with discontinuities in the state or in the derivatives. We emphasize that for all test cases the time step was only restricted by the standard CFL stability condition based on the flux and *not* by the stiffness of the source term.

At this point, we would like to summarize the advantages and the disadvantages of our proposed ADER-FV scheme for hyperbolic systems with stiff source terms. Among the clear advantages of our scheme is the fact that it can reach any desired order of accuracy greater or equal two in space and time simultaneously. To our knowledge, this has not yet been achieved by any other numerical method for hyperbolic systems with stiff source terms. Furthermore, the unsplit finite volume discretization (9) mimics the underlying physics of the governing equation since it is based directly on an integral formulation of the governing PDE (6). The same is true for the (also unsplit) local space–time DG scheme, which directly solves a weak formulation of the local initial value problem (6) in space–time. Since the local space–time DG scheme can be solved individually for each element $\mathcal{Q}_i$ we suppose that for this particular purpose it is easier to solve than a classical globally implicit space–time DG scheme [66] that must take into account all $Q_i \in \Omega$. Numerical evidence has shown that our scheme seems to be consistent with the stiff limit of the governing PDE for a large number of test problems. However, a clear disadvantage of our proposed method is the high computational effort associated with the Newton algorithm that has to be used in the case of nonlinear systems. Compared to the rest of the algorithm, the Newton solver is by far the most expensive part of the scheme. Future work has to be done to make the Newton algorithm for the nonlinear case more efficient and robust. Other, more advanced, techniques can be tried in the future such as inexact Newton solvers based on GMRES with appropriate preconditioning. Seen from a theoretical point of view, another disadvantage of our scheme may be the fact that the first-order version of the method does not work since it does not provide the correct coupling of source terms and fluxes which only comes in via a higher-order discretization in space and time.

Further extensions and applications of the proposed ADER-FV schemes for stiff problems will concern the extension to multiple space dimensions and the application to two-fluid flow. Of particular interest will be the application to colliding plasma flows with stiff friction and temperature relaxation. Further applications may also involve chemically reacting flows.

Acknowledgements

The first author was funded by a post-doctoral grant of the *Deutsche Forschungsgemeinschaft* (DFG) in the framework of the *DFG Forschungsstipendium* (DU 1107/1-1). The second author was funded by a grant of the French *Commissariat à l'Energie Atomique* (CEA) in the framework of his PhD thesis. The constructive comments of the referees have been highly appreciated.

Appendix A. Reconstruction basis functions

The rescaled Legendre polynomials, which constitute an orthogonal basis on the unit interval $I = [0; 1]$, are given up to polynomial degree $M = 5$ by

$$
\begin{aligned}
\Psi_0(\xi) &= 1, \\
\Psi_1(\xi) &= 2\xi - 1, \\
\Psi_2(\xi) &= 6\xi^2 - 6\xi + 1, \\
\Psi_3(\xi) &= 20\xi^3 - 30\xi^2 + 12\xi - 1, \\
\Psi_4(\xi) &= 70\xi^4 - 140\xi^3 + 90\xi^2 - 20\xi + 1, \\
\Psi_5(\xi) &= 252\xi^5 - 630\xi^4 + 560\xi^3 - 210\xi^2 + 30\xi - 1.
\end{aligned} \tag{A.1}
$$

Appendix B. Mass-, flux- and stiffness matrices for the local space–time DG method for the linear case

For polynomial degree $M = 1$, the mass matrix M_{kl} and the time flux matrices F^0_{kl} and F^1_{kl} of the local space–time discontinuous Galerkin scheme are

$$
M_{kl} = \begin{pmatrix} 1 & 0 & 0 & 0 \\ 0 & \frac{1}{3} & 0 & 0 \\ 0 & 0 & \frac{1}{3} & 0 \\ 0 & 0 & 0 & \frac{1}{9} \end{pmatrix}, \quad
F^0_{kl} = \begin{pmatrix} 1 & 0 \\ 0 & \frac{1}{3} \\ -1 & 0 \\ 0 & -\frac{1}{3} \end{pmatrix}, \quad
F^1_{kl} = \begin{pmatrix} 1 & 0 & 1 & 0 \\ 0 & \frac{1}{3} & 0 & \frac{1}{3} \\ 1 & 0 & 1 & 0 \\ 0 & \frac{1}{3} & 0 & \frac{1}{3} \end{pmatrix} \tag{B.1}
$$

and the temporal and spatial stiffness matrices K^τ_{kl} and K^ξ_{kl} are given by

$$
K^\tau_{kl} = \begin{pmatrix} 0 & 0 & 0 & 0 \\ 0 & 0 & 0 & 0 \\ 2 & 0 & 0 & 0 \\ 0 & \frac{2}{3} & 0 & 0 \end{pmatrix}, \quad
K^\xi_{kl} = \begin{pmatrix} 0 & 2 & 0 & 0 \\ 0 & 0 & 0 & 0 \\ 0 & 0 & 0 & \frac{2}{3} \\ 0 & 0 & 0 & 0 \end{pmatrix}. \tag{B.2}
$$

For polynomial degree $M = 2$, these matrices become

$$
M_{kl} = \begin{pmatrix}
1 & 0 & 0 & 0 & 0 & 0 & 0 & 0 & 0 \\
0 & \frac{1}{3} & 0 & 0 & 0 & 0 & 0 & 0 & 0 \\
0 & 0 & \frac{1}{5} & 0 & 0 & 0 & 0 & 0 & 0 \\
0 & 0 & 0 & \frac{1}{3} & 0 & 0 & 0 & 0 & 0 \\
0 & 0 & 0 & 0 & \frac{1}{9} & 0 & 0 & 0 & 0 \\
0 & 0 & 0 & 0 & 0 & \frac{1}{15} & 0 & 0 & 0 \\
0 & 0 & 0 & 0 & 0 & 0 & \frac{1}{5} & 0 & 0 \\
0 & 0 & 0 & 0 & 0 & 0 & 0 & \frac{1}{15} & 0 \\
0 & 0 & 0 & 0 & 0 & 0 & 0 & 0 & \frac{1}{25}
\end{pmatrix}, \tag{B.3}
$$

$$
F^0_{kl} = \begin{pmatrix}
1 & 0 & 0 \\
0 & \frac{1}{3} & 0 \\
0 & 0 & \frac{1}{5} \\
-1 & 0 & 0 \\
0 & -\frac{1}{3} & 0 \\
0 & 0 & -\frac{1}{5} \\
1 & 0 & 0 \\
0 & \frac{1}{3} & 0 \\
0 & 0 & \frac{1}{5}
\end{pmatrix}, \quad
F^1_{kl} = \begin{pmatrix}
1 & 0 & 0 & 1 & 0 & 0 & 1 & 0 & 0 \\
0 & \frac{1}{3} & 0 & 0 & \frac{1}{3} & 0 & 0 & \frac{1}{3} & 0 \\
0 & 0 & \frac{1}{5} & 0 & 0 & \frac{1}{5} & 0 & 0 & \frac{1}{5} \\
1 & 0 & 0 & 1 & 0 & 0 & 1 & 0 & 0 \\
0 & \frac{1}{3} & 0 & 0 & \frac{1}{3} & 0 & 0 & \frac{1}{3} & 0 \\
0 & 0 & \frac{1}{5} & 0 & 0 & \frac{1}{5} & 0 & 0 & \frac{1}{5} \\
1 & 0 & 0 & 1 & 0 & 0 & 1 & 0 & 0 \\
0 & \frac{1}{3} & 0 & 0 & \frac{1}{3} & 0 & 0 & \frac{1}{3} & 0 \\
0 & 0 & \frac{1}{5} & 0 & 0 & \frac{1}{5} & 0 & 0 & \frac{1}{5}
\end{pmatrix}, \tag{B.4}
$$

$$K_{kl}^{\tau} = \begin{pmatrix} 0 & 0 & 0 & 0 & 0 & 0 & 0 & 0 & 0 \\ 0 & 0 & 0 & 0 & 0 & 0 & 0 & 0 & 0 \\ 0 & 0 & 0 & 0 & 0 & 0 & 0 & 0 & 0 \\ 2 & 0 & 0 & 0 & 0 & 0 & 0 & 0 & 0 \\ 0 & \frac{2}{3} & 0 & 0 & 0 & 0 & 0 & 0 & 0 \\ 0 & 0 & \frac{2}{5} & 0 & 0 & 0 & 0 & 0 & 0 \\ 0 & 0 & 0 & 2 & 0 & 0 & 0 & 0 & 0 \\ 0 & 0 & 0 & 0 & \frac{2}{3} & 0 & 0 & 0 & 0 \\ 0 & 0 & 0 & 0 & 0 & \frac{2}{5} & 0 & 0 & 0 \end{pmatrix}, \quad K_{kl}^{\xi} = \begin{pmatrix} 0 & 2 & 0 & 0 & 0 & 0 & 0 & 0 & 0 \\ 0 & 0 & 2 & 0 & 0 & 0 & 0 & 0 & 0 \\ 0 & 0 & 0 & 0 & 0 & 0 & 0 & 0 & 0 \\ 0 & 0 & 0 & 0 & \frac{2}{3} & 0 & 0 & 0 & 0 \\ 0 & 0 & 0 & 0 & 0 & \frac{2}{3} & 0 & 0 & 0 \\ 0 & 0 & 0 & 0 & 0 & 0 & 0 & 0 & 0 \\ 0 & 0 & 0 & 0 & 0 & 0 & 0 & \frac{2}{5} & 0 \\ 0 & 0 & 0 & 0 & 0 & 0 & 0 & 0 & \frac{2}{5} \\ 0 & 0 & 0 & 0 & 0 & 0 & 0 & 0 & 0 \end{pmatrix}. \tag{B.5}$$

Appendix C. Asymptotic preserving property of the local space–time DG scheme

In this appendix, we show that the local space–time discontinuous Galerkin scheme (46) when applied to the linear system (56) has the correct behaviour in the stiff limit, i.e. that it has the so-called asymptotic preserving (AP) property, see [34,23]. We therefore apply the scheme (46) to the system (56) with $u_h \in V_h$, $v_h \in V_h$, $\alpha(u) = 1$ and the small positive parameter $\epsilon = 1/v > 0$:

$$\begin{aligned} &[\Phi_k, u_h]_{t^{n+1}} - [\Phi_k, w_u]_{t^n} - \left\langle \frac{\partial}{\partial t}\Phi_k, u_h \right\rangle + \left\langle \Phi_k, \frac{\partial}{\partial x} v_h \right\rangle = 0, \\ &[\Phi_k, v_h]_{t^{n+1}} - [\Phi_k, w_v]_{t^n} - \left\langle \frac{\partial}{\partial t}\Phi_k, v_h \right\rangle + \left\langle \Phi_k, \frac{\partial}{\partial x} u_h \right\rangle = -\frac{1}{\epsilon}\langle \Phi, v_h \rangle. \end{aligned} \tag{C.1}$$

Here, w_u and w_v denote the reconstruction polynomials at time t^n for the variables u and v, respectively, and the scalar products $[f, g]_\tau$ and $\langle f, g \rangle$ are supposed to be computed in physical space. Let now $u_d \in V_h$ be the discrete solution of the local space–time DG scheme applied to the linear heat equation (60), which is the asymptotic limit of (56) for $\epsilon \to 0$:

$$[\Phi_k, u_d]_{t^{n+1}} - [\Phi_k, w_u]_{t^n} - \left\langle \frac{\partial}{\partial t}\Phi_k, u_d \right\rangle = \epsilon \left\langle \Phi_k, \frac{\partial^2}{\partial x^2} u_d \right\rangle. \tag{C.2}$$

Eq. (C.2) only makes sense for at least piecewise quadratic approximations. Under this assumption on V_h we will show that $u_h \to u_d$ for $\epsilon \to 0$. This is done using an asymptotic expansion of the discrete solution v_h as

$$v_h = v_0 + \epsilon^1 v_1 + \epsilon^2 v_2 + \mathcal{O}(\epsilon^3) \tag{C.3}$$

with $v_0 \in V_h$, $v_1 \in V_h$ and $v_2 \in V_h$.

Inserting (C.3) into (C.1) and retaining only terms up to power ϵ^1 yields

$$\begin{aligned} &[\Phi_k, u_h]_{t^{n+1}} - [\Phi_k, w_u]_{t^n} - \left\langle \frac{\partial}{\partial t}\Phi_k, u_h \right\rangle + \left\langle \Phi_k, \frac{\partial}{\partial x}(v_0 + \epsilon v_1) \right\rangle = 0, \\ &[\Phi_k, v_0 + \epsilon v_1]_{t^{n+1}} - [\Phi_k, w_v]_{t^n} - \left\langle \frac{\partial}{\partial t}\Phi_k, v_0 + \epsilon v_1 \right\rangle + \left\langle \Phi_k, \frac{\partial}{\partial x} u_h \right\rangle = -\frac{1}{\epsilon}\langle \Phi_k, v_0 + \epsilon v_1 + \epsilon^2 v_2 \rangle \quad \forall \Phi_k \in V_h. \end{aligned} \tag{C.4}$$

In (C.4), the leading power ϵ^{-1} yields the condition

$$\langle \Phi_k, v_0 \rangle = 0 \quad \forall \Phi_k \in V_h. \tag{C.5}$$

Since $\Phi_k \in V_h$ and $v_0 \in V_h$, we obtain immediately the result

$$v_0 = 0. \tag{C.6}$$

This condition is necessary to obtain a bounded solution for v_h. The terms of order ϵ^0 in (C.4) yield together with (C.6) the condition

$$\left\langle \Phi_k, \frac{\partial}{\partial x} u_h \right\rangle - [\Phi_k, w_v]_0 = -\langle \Phi_k, v_1 \rangle \quad \forall \Phi_k \in V_h. \tag{C.7}$$

Since $v_0 = 0$, the numerical solution v_h is of the order $\mathcal{O}(\epsilon)$, even if the initial condition w_v was of the order $\mathcal{O}(1)$. If we suppose to do at least two time-steps of the local space–time DG scheme, where the initial condition of the second time step is given by the boundary extrapolated data at local time $\tau = 1$ of the first time step, we can suppose w_v to be of the order $\mathcal{O}(\epsilon)$ and neglect it in (C.7) to obtain

$$\left\langle \Phi_k, \frac{\partial}{\partial x} u_h \right\rangle = -\langle \Phi_k, v_1 \rangle \quad \forall \Phi_k \in V_h. \tag{C.8}$$

Since $u_h \in V_h$, $\Phi_k \in V_h$ and $v_1 \in V_h$, we also obtain the relation

$$\left\langle \Phi_k, \frac{\partial^2}{\partial x^2} u_h \right\rangle = -\left\langle \Phi_k, \frac{\partial}{\partial x} v_1 \right\rangle \quad \forall \Phi_k \in V_h, \tag{C.9}$$

which is non-trivial only for polynomials of degree greater or equal two. Using (C.9), (C.3) and (C.6) we then obtain from (C.4) the equation

$$[\Phi_k, u_h]_{t^{n+1}} - [\Phi_k, w_u]_{t^n} - \left\langle \frac{\partial}{\partial t} \Phi_k, u_h \right\rangle = \epsilon \left\langle \Phi_k, \frac{\partial^2}{\partial x^2} u_h \right\rangle, \tag{C.10}$$

which is the same weak form of the local space–time DG scheme as derived directly for the diffusion equation (C.2). Hence, the formal asymptotic expansion of the local space–time DG scheme shows us that it has the AP property in the sense of [34] for polynomial approximation spaces of degree greater or equal two.

References

[1] W. Bao, S. Jin, Error estimates on the random projection methods for hyperbolic conservation laws with stiff reaction terms, Applied Numerical Mathematics 43 (2002) 315–333.

[2] F. Béreux, Zero-relaxation limit versus operator splitting for two-phase fluid flow computations, Computer Methods in Applied Mechanics and Engineering 133 (1996) 93–124.

[3] A. Bermudez, M.E. Vazquez, Upwind methods for hyperbolic conservation laws with source terms, Computers and Fluids 23 (8) (1994) 1049–1071.

[4] R. Botchorishvili, B. Perthame, A. Vasseur, Equilibrium schemes for scalar conservation laws with stiff sources, Mathematics of Computation 72 (241) (2001) 131–157.

[5] N. Botta, R. Klein, S. Langenberg, S. Lützenkirchen, Well balanced finite volume methods for nearly hydrostatic flows, Journal of Computational Physics 196 (2004) 539–565.

[6] F. Bouchut, H. Ounaissa, B. Perthame, Upwinding of source term at interfaces for Euler equations with high friction, Computers and Mathematics with Applications 53 (2007) 361–375.

[7] A. Bourlioux, A.J. Majda, V. Roytburd, One-dimensional front tracking based on high resolution wave propagation methods, SIAM Journal on Applied Mathematics 51 (1991) 303–343.

[8] C. Buet, B. Després, Asymptotic preserving and positive schemes for radiation hydrodynamics, Journal of Computational Physics 215 (2) (2006) 717–740.

[9] E. Burman, L. Sainsaulieu, Numerical analysis of two operator splitting methods for an hyperbolic system of conservation laws with stiff relaxation, Computer Methods in Applied Mechanics and Engineering 128 (1995) 291–314.

[10] R.E. Caflish, S. Jin, G. Russo, Uniformly accurate schemes for hyperbolic systems with relaxation, SIAM Journal on Numerical Analysis 34 (1997) 246–281.

[11] M. Castro, J.M. Gallardo, C. Pares, High order finite volume schemes based on reconstruction of states for solving hyperbolic systems with nonconservative products, applications to shallow-water systems, Mathematics of Computation 75 (2006) 1103–1134.

[12] G.Q. Chen, C.D. Levermore, T.P. Liu, Hyperbolic conservation laws with stiff relaxation terms and entropy, Communications on Pure and Applied Mathematics 47 (6) (1994) 787–830.

[13] M. Dumbser, Arbitrary High Order Schemes for the Solution of Hyperbolic Conservation Laws in Complex Domains, Shaker Verlag, Aachen, 2005.

[14] M. Dumbser, M. Käser, Arbitrary high order non-oscillatory finite volume schemes on unstructured meshes for linear hyperbolic systems, Journal of Computational Physics 221 (2007) 693–723.

[15] M. Dumbser, M. Käser, V.A. Titarev, E.F. Toro, Quadrature-free non-oscillatory finite volume schemes on unstructured meshes for nonlinear hyperbolic systems, Journal of Computational Physics 226 (2007) 204–243.

[16] M. Dumbser, C.D. Munz, Building blocks for arbitrary high order discontinuous Galerkin schemes, Journal of Scientific Computing 27 (2006) 215–230.

[17] M. Dumbser, T. Schwartzkopff, C.D. Munz, Arbitrary high order finite volume schemes for linear wave propagation, in: Computational Science and High Performance Computing II, Notes on Numerical Fluid Mechanics and Multidisciplinary Design (NNFM), Springer-Verlag, Berlin, Heidelberg, 2006, pp. 129–144.

[18] B. Einfeldt, On Godunov-type methods for gas dynamics, SIAM Journal on Numerical Analysis 25 (1988) 294–318.
[19] B. Einfeldt, C.D. Munz, P.L. Roe, B. Sjgreen, On Godunov-type methods near low densities, Journal of Computational Physics 92 (1991) 273–295.
[20] B. Engquist, S. Osher, One sided difference approximations for nonlinear conservation laws, Mathematics of Computation 36 (1981) 321–351.
[21] J. Glimm, G. Marshall, B. Plohr, A generalized Riemann problem for quasi-one-dimensional gas flows, Advances in Applied Mathematics 5 (1984) 1–30.
[22] S.K. Godunov, Finite difference methods for the computation of discontinuous solutions of the equations of fluid dynamics, Mathematics of the USSR. Sbornik 47 (1959) 271–306.
[23] F. Golse, S. Jin, C.D. Levermore, The convergence of numerical transfer schemes in diffusive regimes. I: The discrete-ordinate method, SIAM Journal on Numerical Analysis 36 (1999) 1333–1369.
[24] L. Gosse, A well-balanced flux-vector splitting scheme designed for hyperbolic systems of conservation laws with source terms, Computers and Mathematics with Applications 39 (2000) 135–159.
[25] L. Gosse, G. Toscani, Asymptotic-preserving and well-balanced schemes for radiative transfer and the Rosseland approximation, Numerische Mathematik 98 (2) (2004) 223–250.
[26] J.M. Greenberg, A.Y. LeRoux, A well-balanced scheme for the numerical processing of source terms in hyperbolic equations, SIAM Journal on Numerical Analysis 33 (1) (1996) 1–16.
[27] A. Harten, B. Engquist, S. Osher, S. Chakravarthy, Uniformly high order essentially non-oscillatory schemes, III, Journal of Computational Physics 71 (1987) 231–303.
[28] A. Harten, P.D. Lax, B. van Leer, On upstream differencing and Godunov-type schemes for hyperbolic conservation laws, SIAM Review 25 (1) (1983) 35–61.
[29] C. Helzel, R.J. LeVeque, G. Warnecke, Modified fractional step method for the accurate approximation of detonation waves, SIAM Journal on Scientific Computing 22 (2000) 1489–1510.
[30] L. Hsiao, T.P. Liu, Convergence to nonlinear diffusion waves for solutions of a system of hyperbolic conservation laws with damping, Communications in Mathematical Physics 143 (1992) 599–605.
[31] F. Huang, P. Marcati, R. Pan, Convergence to the Barenblatt solution for the compressible Euler equations with damping and vacuum, Archive for Rational Mechanics and Analysis 176 (2005) 1–24.
[32] G.-S. Jiang, C.W. Shu, Efficient implementation of weighted ENO schemes, Journal of Computational Physics (1996) 202–228.
[33] S. Jin, Runge–Kutta methods for hyperbolic conservation laws with stiff relaxation terms, Journal of Computational Physics 122 (1) (1995) 51–67.
[34] S. Jin, Efficient asymptotic-preserving (ap) schemes for some multiscale kinetic equations, SIAM Journal on Scientific Computing 21 (1999) 441–454.
[35] S. Jin, A steady-state capturing method for hyperbolic systems with geometrical source terms, Mathematical Modelling and Numerical Analysis 35 (4) (2001) 631–645.
[36] S. Jin, C.D. Levermore, Numerical schemes for hyperbolic conservation laws with stiff relaxation terms, Journal of Computational Physics 126 (2) (1996) 449–467.
[37] S. Jin, Z. Xin, The relaxation schemes for systems of conservation laws in arbitrary space dimensions, Communications on Pure and Applied Mathematics 48 (1995) 235–277.
[38] P. LeFloch, P.A. Raviart, An asymptotic expansion for the solution of the generalized Riemann problem, Part I: general theory, Annales de l'Institut Henri Poincaré 5 (2) (1988) 179–207.
[39] A.Y. LeRoux, Riemann solvers for some hyperbolic problems with a source term, in: ESAIM: Proceedings CANUM, vol. 6, 1998, pp. 75–90.
[40] R.J. LeVeque, K.-M. Shyue, One-dimensional front tracking based on high resolution wave propagation methods, SIAM Journal on Scientific Computing 16 (1995) 348–377.
[41] R.J. LeVeque, H.C. Yee, A study of numerical methods for hyperbolic conservation laws with stiff source terms, Journal of Computational Physics 86 (1) (1990) 187–210.
[42] X.D. Liu, S. Osher, T. Chan, Weighted essentially non-oscillatory schemes, Journal of Computational Physics 115 (1994) 200–212.
[43] R.B. Lowrie, J.E. Morel, Methods for hyperbolic systems with stiff relaxation, International Journal for Numerical Methods in Fluids 40 (2002) 413–423.
[44] F. Miniati, P. Colella, A modified higher order Godunov's scheme for stiff source conservative hydrodynamics, Journal of Computational Physics 224 (2) (2007) 519–538.
[45] G. Naldi, L. Pareschi, Numerical schemes for hyperbolic systems of conservation laws with stiff diffusive relaxation, SIAM Journal on Numerical Analysis 37 (4) (2000) 1246–1270.
[46] S. Osher, F. Solomon, Upwind difference schemes for hyperbolic conservation laws, Mathematics of Computation 38 (1982) 339–374.
[47] L. Pareschi, G. Russo, Implicit-explicit Runge–Kutta schemes for stiff systems of differential equations, Advances in the Theory of Computational Mathematics 3 (2000) 269–288.
[48] R.B. Pember, Numerical methods for hyperbolic conservation laws with stiff relaxation, I. Spurious solutions, SIAM Journal on Applied Mathematics 53 (5) (1993) 1293–1330.
[49] R.B. Pember, Numerical methods for hyperbolic conservation laws with stiff relaxation. II. Higher order Godunov methods, SIAM Journal on Scientific Computing 14 (4) (1993) 824–859.
[50] B. Perthame, C. Simeoni, Convergence of the upwind interface source method for hyperbolic conservation laws, in: T. Hou, E. Tadmor (Eds.), Proceedings of Hyp2002, Springer, 2003.

[51] W.H. Press, S.A. Teukolsky, W.T. Vetterling, B.P. Flannery, Numerical Recipes in Fortran 77, vol. 1, Cambridge University Press, 1996.
[52] J. Qiu, M. Dumbser, C.W. Shu, The discontinuous Galerkin method with Lax–Wendroff type time discretizations, Computer Methods in Applied Mechanics and Engineering 194 (2005) 4528–4543.
[53] J. Qiu, C.W. Shu, Finite difference WENO schemes with Lax–Wendroff type time discretization, SIAM Journal on Scientific Computing 24 (6) (2003) 2185–2198.
[54] P.L. Roe, Approximate Riemann solvers, parameter vectors, and difference schemes, Journal of Computational Physics 43 (1981) 357–372.
[55] T. Schwartzkopff, M. Dumbser, C.D. Munz, Fast high order ADER schemes for linear hyperbolic equations, Journal of Computational Physics 197 (2004) 532–539.
[56] C.W. Shu, S. Osher, Efficient implementation of essentially non-oscillatory shock capturing schemes II, Journal of Computational Physics 83 (1989) 32–78.
[57] G. Strang, On the construction and comparison of difference schemes, SIAM Journal on Numerical Analysis 5 (3) (1968) 506–517.
[58] A.H. Stroud, Approximate Calculation of Multiple Integrals, Prentice-Hall Inc., Englewood Cliffs, New Jersey, 1971.
[59] V.A. Titarev, E.F. Toro, ADER: arbitrary high order Godunov approach, Journal of Scientific Computing 17 (1–4) (2002) 609–618, December.
[60] V.A. Titarev, E.F. Toro, ADER schemes for three-dimensional nonlinear hyperbolic systems, Journal of Computational Physics 204 (2005) 715–736.
[61] E.F. Toro, Riemann Solvers and Numerical Methods for Fluid Dynamics, second ed., Springer, 1999.
[62] E.F. Toro, R.C. Millington, L.A.M. Nejad, Towards very high order Godunov schemes, in: E.F. Toro (Ed.), Godunov Methods. Theory and Applications, Kluwer/Plenum Academic Publishers, 2001, pp. 905–938.
[63] E.F. Toro, M. Spruce, W. Speares, Restoration of the contact surface in the Harten–Lax–van Leer Riemann solver, Journal of Shock Waves 4 (1994) 25–34.
[64] E.F. Toro, V.A. Titarev, Solution of the generalized Riemann problem for advection–reaction equations, Proceedings of the Royal Society of London Series A 458 (2002) 271–281.
[65] E.F. Toro, V.A. Titarev, ADER schemes for scalar hyperbolic conservation laws with source terms in three space dimensions, Journal of Computational Physics 202 (2005) 196–215.
[66] J. van der Vegt, H. van der Ven, Space–time discontinuous Galerkin finite element method with dynamics grid motion for inviscid compressible flows, part I. General formulation, Journal of Computational Physics 182 (2002) 546–585.